https://doi.org/10.5194/esd-2021-30
Preprint. Discussion started: 7 May 2021

Earth System Dynamics Discussions

Accounting for surface waves improves gas flux estimation at high wind speed in a large lake

Pascal Perolo[1], Bieito Fernandez Castro[2,3], Nicolas Escoffier[1], Thibault Lambert[1], Damien Bouffard[4], Marie-Elodie Perga[1]

[1]Institute of Earth Surface Dynamics, University of Lausanne, Lausanne, 1015, Switzerland
[2]Physics of Aquatic Systems Laboratory, Margareth Kamprad Chair, Swiss Federal Institute of Technology Lausanne, Lausanne, 1015, Switzerland
[3]Ocean and Earth Science, University of Southampton, National Oceanography Centre, Southampton, SO14 3ZH, United Kingdom
[4]Eawag, Swiss Federal Institute of Aquatic Science and Technology, Surface Waters – Research Management, Kastanienbaum, 6047, Switzerland

Correspondence to: Pascal Perolo (pascal.perolo@unil.ch)

Abstract. The gas transfer velocity (k) is a major source of uncertainty when assessing the magnitude of lake gas exchange with the atmosphere. For the diversity of existing empirical and process-based k models, the transfer velocity increases with the level of turbulence near the air-water interface. However, predictions for k can vary by a factor of 2 among different models. Near-surface turbulence results from the action of wind shear, surface waves and buoyancy-driven convection. Wind shear has long been identified as a key driver, while recent lake studies have shifted the focus towards the role of convection, particularly in small lakes. In large lakes, wind fetch can however be long enough to generate surface waves and contribute to enhance gas transfer, as widely recognised in oceanographic studies. Here, field values for gas transfer velocity were computed in a large hardwater lake, Lake Geneva, from CO_2 fluxes measured with an automated (forced diffusion) flux chamber and CO_2 partial pressure measured with high frequency sensors. k estimates were compared to a set of reference limnological and oceanic k models. Our analysis reveals that accounting for surface waves generated during windy events significantly improves the accuracy of k estimates in this large lake. The improved k model is then used to compute k over a one-year time-period. Results show that episodic extreme events with surface waves (6 % occurrence, significant wave height > 0.4 m) can generate more than 20 % of annual cumulative k and more than 25 % of annual net CO_2 fluxes in Lake Geneva. We conclude that for lakes whose fetch can exceed 15 km, k-models need to integrate the effect of surface waves.

1 Introduction

Lakes are universally regarded as significant sources of CO_2 to the atmosphere, however, the accurate quantification of the magnitude of such emissions remains to date challenging (Cole et al., 2007; Tranvik et al., 2009; Raymond et al., 2013). While CO_2 fluxes can be directly measured with floating chamber or eddy covariance systems (Vachon et al., 2010; Vesala et al., 2006), these approaches suffer from limited time and space integration (from minutes to hours, and centimetres to metres;

https://doi.org/10.5194/esd-2021-30
Preprint. Discussion started: 7 May 2021


Earth System Dynamics Discussions

Klaus and Vachon, 2020). Long-term direct flux measurements are thereby mostly restricted to small lakes (Huotari et al., 2011) and fluxes remain mostly estimated with models. CO_2 fluxes at the surface of lakes operate through a net diffusive transport, therefore obeying the Fick's first law:

$$F = k\alpha\Delta pCO_2 \ , \quad (1)$$

where F (mol m^{-2} s^{-1} but often expressed as µmol cm^{-2} h^{-1}) is the CO_2 gas flux, α is the CO_2 solubility coefficient (µmol cm^{-3} μatm^{-1}), ΔpCO_2 is the gradient of partial pressure of CO_2 (pCO_2) between the water and the atmosphere corrected for altitude (µatm); and k is the gas transfer velocity (cm h^{-1}).

Lake carbon emissions are therefore primarily driven by the gradient of partial pressure of CO_2 between the surface lake water and the atmosphere, but the gas-transfer velocity controls the rate of CO_2 exchange across the lake-atmosphere interface. Assessing the amount of lake CO_2 emissions to the atmosphere has been a major issue, starting with the Cole and al's 1998 seminal paper, with debates regarding both the representativeness of the measurements and the optimal conceptual model for air-water gas transfer (e.g., MacIntyre et al., 2001; Borges et al., 2004). As recent developments in sensor technologies allow continuous and accurate measurements of aqueous CO_2 concentrations, the gas transfer velocity remains, to date, the main source of uncertainties, which hinders attempts to achieve full carbon budgets (Dugan et al., 2016) or to quantify greenhouse gas emissions by lakes, at local, regional, or worldwide scales (Maberly et al., 2012; Raymond et al., 2013; Engel et al., 2018).

k is inherently tied to turbulent mixing within the surface boundary layer, which enhances the diffusive gas exchange by renewing the surface mass content (Zappa et al., 2007). At the lake-atmosphere interface, turbulent mixing is the product of wind shear, buoyancy flux, and wind-driven surface waves, whose effect can be split into wave action and wave breaking, the latter producing air bubble and water spray (Fig. 1; Wüest and Lorke, 2003, Soloviev et al., 2007). Regarding the prominent role of wind action on surface turbulence, first quantitative models have empirically scaled k to wind-speed (referenced at a 10 m height; U_{10}), as a proxy for the level of wind-driven turbulence (Fig. 1; Cole and Caraco, 1998; Crusius and Wanninkhof, 2003). The parameterizations of the k-wind relationships vary between authors (e.g., Klaus and Vachon 2020), as a likely consequence of the local characteristics of the lakes used in the calibration datasets (Table 1). Yet, all studies suggested a polynomial relationship between U_{10} and k with order larger than unity. Further development of empirical models integrated the lake surface area as a second parameter in the k-wind relationships, to account for the role of the fetch length for wind action (Vachon and Prairie, 2013). Generally, empirical wind-based models tend to underestimate fluxes, especially at low-wind speed (e.g., Schubert et al., 2012; Heiskanen et al., 2014; Mammarella et al., 2015) where turbulent mixing through buoyancy flux is expected to take over wind shear. Besides, these empirical models require a proper calibration each time they are applied in a new system with different characteristics, i.e., a new set of lakes and/or meteorological conditions (Klaus and Vachon, 2020), hence limiting their universal applicability.

Figure 1

https://doi.org/10.5194/esd-2021-30
Preprint. Discussion started: 7 May 2021


Earth System Dynamics Discussions

In parallel to empirical wind-based models, process-based models attempt to link k directly to near-surface turbulence. The surface renewal model (SRM) is one of the first, and still most widely used, theories (Danckwerts 1951; Lamont and Scott, 1970) with k depending on the product of the turbulent kinetic energy dissipation rate (ε) and the kinematic viscosity of water (υ), both to a power of one quarter as follows:

$$k = a_1(\varepsilon\upsilon)^{1/4}Sc^{-1/2}\,, \quad (2)$$

with a_1 a calibration constant parameter and Sc, the Schmidt number. Recently Lorke and Peeters (2006) and Katul and Liu (2017) demonstrated that this relationship, to which different approaches converge, can be seen as a universal scaling. As opposed to the practical empirical models presented above, process-based models have the potential to predict k using the turbulent dissipation rate over a wide range of environmental conditions extending beyond those encountered in the calibration dataset (Zappa et al., 2007). As for lakes, SRM k-models have so far considered the friction velocity at the water side ($u_{,wat}$) and the turbulence created by thermal convection using the buoyancy flux at the surface (B_0) (Fig. 1; Eugster et al., 2003; MacIntyre et al., 2010; Read et al., 2012; Tedford et al., 2014; Heiskanen et al., 2014). Noteworthily, the SRM approach leads to k being related to $u_{,wat}$ (or U_{10}) to the first order (Wanninkhof, 1992; Lorke and Peeters 2006; see also Material and Methods section), while empirical models described above predict a higher order polynomial relationship. This inconsistency is tentatively solved in oceanography by adding another source of gas exchange associated with wind-waves whitecaps. Early gas flux parameterization already accounted for wind and buoyancy-driven turbulence together with surface waves (Fig. 1; Woolf et al., 1997; Soloviev et al., 2007; Fairall et al., 2011). Yet, the buoyancy-driven contribution can often be neglected in oceanography, and recent efforts have been dedicated to a better parameterization of the bubble enhancement term (Fig. 1; Deike and Melville, 2018). In lakes, wind fetch can be long enough to generate surface waves (Wanninkhof, 1992; Frost and Upstill-Goddard, 2002; Borges et al., 2004; Guérin et al., 2007), thus implying that surface waves could be a significant driver of k and subsequent CO_2 fluxes (Schilder et al., 2013; Vachon and Prairie, 2013). Insofar, the role of surface waves has been essentially accounted empirically in lake k-models, through the polynomial scaling to U_{10} in wind-based models, and most often neglected in studies using process-based parameterizations (mainly SRM) (e.g., Read et al., 2012). While this approximation may be appropriate for small-shielded lakes, it is likely to be insufficient in larger, long-fetched lakes.

Herein, we aim to identify the most adequate k-model for Lake Geneva, a large clear hardwater lake in the Swiss Alps, to assess k values over a full annual cycle. We compare the performances of different models of gas transfer velocity, in their original or slightly modified published formulations from the limnological and oceanic literatures. This set of models includes different levels of complexity, ranging from empirical models integrating wind speed and lake size, to process-based models including wind shear, convection, and surface waves. Continuous ΔpCO_2 measurements by in situ automated sensors and CO_2 fluxes, obtained from a new generation of automated (forced diffusion) flux chamber, were collected during specific periods of intensive field survey covering a wide range of natural conditions. Empirical k values computed from chamber data are then compared to outputs from the different k-models. Owing to the size of Lake Geneva, we anticipate that models accounting,

https://doi.org/10.5194/esd-2021-30
Preprint. Discussion started: 7 May 2021

implicitly or explicitly, for the four key exchange drivers (i.e., wind shear, convective mixing, wave action and bubble formation) will show the highest accuracy and precision in their estimation of *k* and that a precise integration of surface wave effects in such a large system should enhance model predictions. Thereafter, the relative distribution of these components is computed over a full year and analysed in the scope of the temporal variability of the gas transfer velocity. Finally, we expect that extreme wind and associated wave events should contribute disproportionately to accumulated *k* values over the year. In such a case, episodic weather events could generate large CO_2 fluxes over very short timescales that should be accounted for when computing annual CO_2 emission budgets.

2 Material and Methods

2.1 Study Site

Lake Geneva is a peri-alpine lake defining part of the Swiss-French border, at 372 m above sea level (46° 26' N; 6° 33' E). Its surface area (582 km^2) and its maximum depth (309 m) make it the largest freshwater body in Western Europe, with a volume of 89 km^3 (Fig. 2). Lake Geneva is monomictic. The two prevailing winds are nearly opposed and come from southwest and northeast respectively (Fig. 2). The lake water has been monthly or fortnightly surveyed from the late 1950's (OLA-IS, AnaEE-France, INRAE of Thonon-les-Bains, CIPEL, Rimet et al., 2020). Surface CO_2 concentrations, as computed from the routine temperature, alkalinity, and pH measurements (Stumm and Morgan, 1981), show a typical seasonal cycle with high, supersaturated values during winter mixing and values below saturation in summer (Perga et al., 2016).

Figure 2

2.2 Field data at LéXPLORE

All field data were collected from the LéXPLORE platform, a 10 m by 10 m pontoon equipped with high-tech instrumentation and installed on Lake Geneva in 2019. LéXPLORE is moored at a 110 m depth, 570 m off the northern lake shore (Fig. 2).

On LéXPLORE, local weather conditions (air temperature, wind speed and direction, relative humidity, short wave radiation and atmospheric pressure) were continuously recorded (10 minutes intervals) by a Campbell Scientific Automatic Weather Station. Lake surface temperature was measured every minute at 50 cm-depth using a Minilog II-T (Vemco, resolution 0.01° C). Partial pressure of water surface CO_2 (pCO_2) was also measured at 50 cm-depth during specific surveys (see flux measurement) using a miniCO_2 sensor (Pro-Oceanus Systems Inc.) with an accuracy of ± 30 ppm. Values of pCO_2 in ppm were converted into µatm following the basic equation correcting for altitude (Russell and Denn, 1972). We therefore assume that the concentration and the temperature are homogeneous over the first 50 centimetres.

Fetch distance (m) from LéXPLORE to the lake shores considering wind direction was computed using data from the Federal Office of Topography online portal (Swisstopo-geoportal: geo.admin.ch). The position of LéXPLORE is particularly relevant

https://doi.org/10.5194/esd-2021-30
Preprint. Discussion started: 7 May 2021


Earth System Dynamics Discussions Open Access EGU

for this study as the fetch ranges from ~0.5 km to ~30 km for the two prevailing winds. Significant wave height, H_s, (in m) was computed after Hasselmann et al. (1973) according to:

$$H_s = 1.6 \cdot 10^{-3} \cdot U_{10} \cdot (Fetch/g)^{1/2}\,, \quad (3)$$

where g is the gravitational constant. This equation is equivalent to the formulation by Carter (1982) that is more widely used in the oceanic literature. Simon (1997) tested the model for significant wave heights in Lake Neuchâtel (a nearby but smaller lake than Lake Geneva) with a fetch distance of 9 km. His results showed that, beyond a critical threshold of wind value (~5 m s^{-1}) wave breaking occurs faster and with a higher probability in the case of not fully developed surface waves. Such waves are characterized by steeper slopes that favour their breaking (Wüest and Lorke, 2003).

The net CO_2 flux at the lake-atmosphere interface, F, was directly measured with an automated (forced diffusion) floating CO_2 flux chamber (eosFD, eosense: environmental gas monitoring; Risk et al., 2011) originally developed for soil flux studies. The flux chamber had a detection limit close to 0.05 µmol cm^{-2} h^{-1} and measured F every 15-minutes in summer and 30-minutes in winter for battery-saving purpose. The standard floating chambers require quiet surface conditions (e.g., Cole et al., 2010; Vachon et al., 2010; Bastviken et al., 2015), thus limiting studies from low to moderate wind speed conditions. One typical problem with floating chambers arises from the possible atmospheric leakage under rough surface. Our flux chamber was specifically conceived to increase stability under windy conditions (Fig. A1). We tested the performance of the floating chamber by comparing the standard deviation of the CO_2 concentrations of the atmosphere and in the chamber estimated from two separated cavities (Fig. A1; Risk et al., 2011). We did not observe any difference in the standard deviation between high and low wind conditions (Fig A3), suggesting that the measured fluxes remained reliable at high wind speed.

We assessed the performances of our flux chamber during 5 specific periods over the annual cycle (i.e., 13th–14th June 2019, 27th–28th August 2019, 1st–5th October 2019, 18th–20th December 2019, and 20th–26th February 2020). To select the most robust dataset to compare with k estimates derived from models, we discarded flux data that were below the detection limit, as well as CO_2 gradients that ranged within the uncertainty of sensors (i.e., ± 20 ppm for air and ± 30 ppm for water leading to ± 50 ppm) (Fig. A2). Accordingly, we were able to retain the most robust data points during the following deployment periods: 18th–20th December 2019 and 20th–26th February 2020. Finally, all these field data were standardized at a 1-hour timestep.

2.3 Computed *k* values from field data

k values (cm h^{-1}) from field observations (k_{obs}) were computed from the gas transfer velocity equation:

$$k_{obs} = F/(\alpha \cdot \Delta pCO_2), \quad (4)$$

where F is the measured CO_2 flux (µmol cm^{-2} h^{-1}), α is the gas solubility coefficient (µmol cm^{-3} µatm^{-1}), which depends on the measured water temperature (Wanninkhof, 1992). ΔpCO_2 is the differential of pCO_2 measured at 0.5 m below the surface

https://doi.org/10.5194/esd-2021-30
Preprint. Discussion started: 7 May 2021


Earth System Dynamics Discussions

(pCO_2^{water}) and pCO_2 at saturation (pCO_2^{sat}) in ppm measured from the flux chamber corrected by altitude (µatm). k_{obs} was then standardized in k_{600} using the dimensionless Schmidt number (Sc) of CO_2 by the equation: $k_{600-obs} = k_{obs} \cdot (600/Sc)^{-1/2}$ (600 for freshwater standardized at 20° C).

2.4 Models for air–water gas transfer velocity

After years of debate, a consensus begins to emerge on the relationship linking *k*, intensity of turbulence and *Sc* (Eq. 2), even when starting from different physical assumptions (see Katul et al., 2018). In this study, we selected six parameterizations widely used in limnology and oceanography combining specific calibration characteristics (Table 1). We first show that they can all be expressed following Eq. (2) for wind shear and convection, despite their different formulations. Then, we develop the effects of surface waves from oceanic models and adapt the wave action for a large lake. The final lake model integrating wave effect is ultimately calibrated using our field data (Table 1).

Table 1

2.4.1 Wind shear

We start with the case where near-surface dynamics are driven by a weak to moderate wind, in absence of heat exchange. In this case, the contribution of surface waves can be neglected and the wind stress ($\tau_0 = \rho_{air} \cdot C_{10} \cdot U_{10}$) is equal to the tangential shear stress ($\tau_t = \rho_{wat} \cdot {u_{*,wat}}^2$). The relationship between ε and the sheared velocity on the water side, $u_{*,wat}$, is then derived from a law-of-the-wall scaling for the velocity profile: $\varepsilon = u_{*,wat}^3/\kappa\, z(0)$ with *K* being the von Kármán constant (= 0.41) and $z(0)$ the thickness of the diffusive boundary layer. This relationship leads to:

$$k_{NB} = a_1 \cdot \left(\nu\, u_{*,wat}^3/\kappa z(0)\right)^{1/4} Sc^{-0.5}\,, \tag{5}$$

The challenge is then to define $z(0)$. Tedford et al. (2014) followed an ad hoc observational approach and chose $z(0)$= 0.15 m, as the shallower depth where ε was measured. In contrast, theoretical studies linked $z(0)$ to the thickness of the diffusive or viscous sublayer (~0.1–1 cm). In line with theory, we scale this layer as $z(0) = c\nu/u_{*,wat}$ (Wüest and Lorke, 2003; Lorke and Peeters, 2006) with *c* as a constant value. Taking *c* = 114 (Soloviev et al., 2007), the thickness of this layer typically ranges from 0.04 to 0.14 m under a wind regime of 10 to 1 m s^{-1}. We therefore modify Eq. (5) as to compute the interfacial (no-bubble, NB) exchange coefficient:

$$k_{NB} = a_1 u_{*,wat} (1/\kappa c)^{1/4} Sc^{-0.5}, \tag{6a}$$

or

$$k_{NB} = a_1 (\rho_{air}/\rho_{wat}) C_{10} U_{10} (1/\kappa c)^{1/4} Sc^{-0.5}\,, \tag{6b}$$

These equations show that the SRM formulation (Soloviev et al., 2007; Read et al., 2012; Table 1 and Fig. B1) is analogous to the COAREG flux algorithm (Fairall et al., 2011), and the formulation used in Deike and Melville (2018) with the sheared

https://doi.org/10.5194/esd-2021-30
Preprint. Discussion started: 7 May 2021


Earth System Dynamics Discussions

velocity on the atmosphere side, $u_{*,atm}$ (Table 1: *DM18*). Indeed, when equating the expression by Deike and Melville (2018):

$$k_{NB} = A_{NB} u_{*,atm} (Sc/600)^{-1/2} = A_{NB} u_{*,wat} (\rho_{wat}/\rho_{atm})^{1/2} (Sc/600)^{-1/2}\,, \quad (7)$$

with (6a), we find that the coefficient a_1 = 0.29 in Soloviev et al., (2007) and Read et al., (2012) is essentially equivalent to the coefficient $A_{NB} = a_1(\kappa c)^{-1/4}(1/600)^{1/2}(\rho_{wat}/\rho_{air})^{-1/2} \approx 1.5 \times 10^{-4}$ in Deike and Melville (2018) (Fig. B1), which in turn was found equal to the coefficient of A = 1.5 in Fairall et al. (2011). These results agree with Lorke and Peeters (2006) who derived a unified relation for interfacial fluxes (air-water and water-sediment) through a linear relationship of $u_{,wat}$ to k, especially at the bottom interface where shear is the only relevant process. Furthermore, Equation 6 has a similar (i.e., quasi-linear) wind-k relationship as the data-driven parameterization from *VP13* but cannot explain the higher order polynomial relationship reported in *CW03* and *CC98*.

2.4.2 Convection

A second source of dissipation at the surface is the convection (ε_c) resulting from surface cooling. The combination of wind shear and free convection near a boundary is described by the Monin-Obukhov similarity theory (MOST) with a general form derived from a turbulent kinetic energy balance (Lombardo and Gregg, 1989; Tedford et al. 2014):

$$\varepsilon(z) = \varepsilon_u(z)\left(c_u + c_c\left\lfloor\frac{z}{L_{MO}}\right\rfloor\right), \quad (8)$$

where L_{MO} is the Monin Obukov length scale defined as $L_{MO} = u_{,wat}^3/\kappa B_0$, including $\varepsilon(z) = c_u \cdot \varepsilon_u + c_c \cdot \varepsilon_c$ in Eq. (2) that can be rearranged as:

$$k_{NB} = a_1\left(\varepsilon_u(c_u + c_c \cdot B_0/\varepsilon_u)^{1/4}\right)Sc^{-1/2}\,, \quad (9)$$

a_1 ranges in the literature from 0.2 to 1.2 (Soloviev et al., 2007; MacIntyre et al., 2010; Tedford et al., 2014; Heiskanen et al. 2014; Winslow et al., 2016), c_u from 0.84 to 1 (Winslow et al., 2016) and c_c from 0.37 to 2.5 (Wyngaard and Coté, 1971; Tedford et al., 2014). Hereafter, we use the following set of values: c_u = 1 and c_c = 1. Fairall et al. (2011) used an essentially equivalent approach but formulated in terms of a Richardson number to describe the partitioning between dissipation from convection and wind shear, expressing the wind shear in terms of the air-side friction velocity: $R_f = B_0 \upsilon/u_{,atm}^4$, which can be integrated into (9) as:

$$k_{NB} = a_1\left(\frac{\rho_{atm}}{\rho_{wat}}\right)^{1/2} u_{,atm}\left(\frac{c_u}{\kappa c}\left(1 + \frac{R_f}{R_{f,c}}\right)\right)^{1/4}\left(\frac{Sc}{600}\right)^{-1/2}\,, \quad (10)$$

with $R_{f,c} = \frac{c_u \rho_{atm}^2}{c_c \rho_{wat}^2 \kappa c}$. The details of this demonstration can be seen in Soloviev and Schlüssel (1994).

https://doi.org/10.5194/esd-2021-30
Preprint. Discussion started: 7 May 2021


Earth System Dynamics Discussions

2.4.3 Wave action

The effect of surface waves is commonly implemented in oceanography but barely considered in limnology. All process-based models rely on the same parameterization of energy dissipation by wind shear and convection. They however differ in how they parameterize energy dissipation by wave action and wave breaking.

The contribution of the wave action (ε_w) is, accordingly, added as a third source of turbulence (Fig. 1). In the presence of surface waves, the balance between τ_t and τ_0 does not hold anymore. Therefore, Soloviev and Schlüssel (1994) added a corrective factor, φ, using the Keulegan number ($Ke = u_{,wat}^3/(gv)$), in order to decrease the component $\tau_t = \tau_0 \cdot \varphi$ where $\varphi = 1/(1 + Ke/Ke_c)$, with the critical Keulegan number (Ke_c) define in Soloviev and Lukas (2006). As a result, the equation for shear-driven dissipation ε_u(z) is:

$$\varepsilon_u(z) = \frac{u_{,wat}^4}{\kappa c v} \cdot \varphi^2 \,, \tag{11}$$

Following this step, the turbulent kinetic energy dissipation rate from wave action (ε_w) is added and defined with the Keulegan number by Soloviev et al. (2007) as:

$$\varepsilon_w = \alpha_W \left(\frac{3}{BS_q}\right)^{1/2} \frac{(Ke/Ke_{cr})^{3/2}}{(1+Ke/Ke_{cr})^{3/2}} \frac{u_{,wat} g}{0.062 \kappa C_T (2\pi A_w)^{3/2}} \frac{\rho_{atm}}{\rho_{wat}} \,, \tag{12}$$

where $C_T = (z_0/H_s)$. z_0 is the surface roughness scale from the water side and the C_T value is set as a constant at 0.6 (More details in Soloviev et al., 2007). This definition does not hold for closed basins because, in the case of incompletely developed waves, the dissipation of energy from wind shear transmitted to the waves is not fully redistributed in the water body (Simon, 1997). Hence, for the application in Lake Geneva, we followed Terray et al. (1996) who defined a varying C_T:

$$C_T = 1.38 \cdot 10^{-4} \left(\frac{U_{10}}{C_p}\right)^{2.66} \,, \tag{13}$$

where C_p is the peak speed of the wave spectrum defined in Deike and Melville (2018) according to Toba (1972, 1978). This leads to $C_T << 1$. This allows to increase the effect of ε_w (inversely proportional to C_T in Eq. 12) on *k*. Here, we used this formulation to adapt the *S07* ocean model for a large lake (closed basin). Henceforth we refer to the adapted uncalibrated and calibrated models as *SD20* and *SD20-fit*, respectively (Table 1). Finally, these three terms of ε (ε_u, ε_c,Λ ε_w) can be added before computing the SRM (Eq. 2) for determining *k*-no bubble (k_{NB}).

2.4.4 Bubble enhancement

Additional deviations from the linear relationship to U_{10} are explained by the gas transfer resulting from bubbles and sprays during wave breaking. This mechanism is accounted for by adding a *k*-bubble (k_B) term to the already mentioned k_{NB}. Soloviev et al. (2007) used the empirical *k*-bubble parameterization from Woolf et al. (1997):

https://doi.org/10.5194/esd-2021-30
Preprint. Discussion started: 7 May 2021


Earth System Dynamics Discussions

$$k_B = W \frac{2450}{O_s\left(1+\frac{1}{(14O_sSc^{-0.5})^{1/1.2}}\right)^{1.2}}, \quad (14)$$

where W is the fractional whitecap coverage only expressed as a function of wind ($3.84 \cdot 10^{-6} \cdot U_{10}^{3.41}$ and O_s is Ostwald gas solubility. This formulation does not take wave height into account (Fig. B1). Nevertheless, a recent study (Deike and Melville, 2018) performed a new numerical process-based parameterization for gas transfer velocity from bubble enhancement considering H_s through the following equation:

$$k_B = \frac{A_B}{O_s} u_{*,atm}^{5/3} (gH_s)^{2/3} \left(\frac{Sc}{600}\right)^{-1/2}, \quad (15)$$

where A_B is an empirical factor with dimension (= 10^{-5} m^{-2} s^2) and O_s defines by the ideal gas constant (R), the surface water temperature (T_0) and, CO_2 solubility coefficient in freshwater (α) (Reichl and Deike, 2020). Then, the gas transfer velocity is expressed as a sum of no-bubble k_{NB} and bubble k_B components (Table 1: *S07*, *DM18*, *SD20, and SD20-fit*) following Keeling (1993) and Woolf et al. (1997, 2005). Our adapted models modified from *S07* (*SD20* and *SD20-fit*) include a refined parameterization of the wave action term ε_w along with the bubble term from *DM18* (*SD20* and *SD20-fit*). In addition, for the model *SD20-fit*, the a_1 parameter of Eq. (2) and the A_B parameter of Eq. (15) were fitted to the k_{600} observations (a_1 = 0.33 and A_B = 3 10^{-5} m^{-2} s^2).

With this review of existing and adapting parameterizations, we show that (i) there is a discrepancy between SRM-based model with shear stress as the only energy source and empirical parameterizations with polynomial (order > 1) wind-based relationship. Such a discrepancy is tentatively resolved by adding the effect of convection and surface waves. (ii) We further highlight that most fitting parameters from the different SRM-based models are in good agreement. (iii) We finally recall that it is possible to provide a unifying parameterization of k with SRM model including wind shear, wind-induced waves, and convection with only a few input parameters such as U_{10}, B_0, and *Fetch*.

3 Results

3.1 Observed and predicted *k*

After quality check, our dataset contains 94 discrete CO_2 flux observations. We first assess the representativeness of our sampling by comparing the survey-specific and annual distributions of the three main inputs for k-models: U_{10} (all models), B_0 during convective periods (*T14*, *S07*, *SD20* & *SD20-fit*) and H_s (*S07*, *DM18*, *SD20* & *SD20-fit*) (Fig. 3; Temporal evolution of these three terms in Fig. C1). From 13th June 2019 to 12th June 2020, the average wind speed over Lake Geneva is 2.9 m s^{-1} with a mode at 2.5 m s^{-1}; very low wind speeds (< 1 m s^{-1}) are encountered 12 % of the year, while high- (> 5 m s^{-1} to very high > 10 m s^{-1}) wind events represent 15 % and 2 % of the year, respectively. The sampling surveys covered the full annual range of U_{10}. Average and modal values of B_0 over the year are close to 0.25 10^{-7} m^2 s^{-3}. However, the sampling covered only

https://doi.org/10.5194/esd-2021-30
Preprint. Discussion started: 7 May 2021


Earth System Dynamics Discussions

the lowest 50 % of the annual distribution and under-samples conditions of potentially strong convection. Considering that the dissipation by buoyancy flux, as parameterized in the process-based models, is already well known in the literature and that it is not the central point of our study, we posit that the under-sampling of B_0 is therefore not expected to significantly affect our analysis. The predicted modal H_s value is 0.15 m over the year. Events of high H_s (> 0.4 m) represent 6 % of the year, with a maximum H_s of 1.1 m. As for U_{10}, the surveys covered the full range of annual H_s.

Figure 3

Observationally based k_{600} are shown with their error bars corresponding to the uncertainties of the pCO_2 in air and in water ($\pm$ 50 ppm) in Fig. 4a. We notice that all the measurements with a wave height > 0.4 m were observed for wind speeds > 5 m s^{-1} and the corresponding k_{600} are located above the linear function (i.e., from a linear regression against wind shear velocity; Fig. B1) scaling k_{600} to u_* (i.e., first order relationship) We then compare the k_{600} observed during the specific surveys to the values computed with all k_{600} models throughout the annual cycle, in relation to U_{10} (Fig. 4b-c). Table 2 provides the root-mean square errors (RMSE) for all model estimates compared to k_{obs} during the flux surveys, (i) for the full dataset (All Wind), and split (ii) for low wind (< 5 m s^{-1}, LW) and (iii) strong wind conditions ($\geq$ 5 m s^{-1}, SW). The three empirical wind-based models only depend on wind (Fig. 4b). Both *CC98* and *CW03* were originally calibrated for small lakes, using a mass balance calibration method (Table 1). However, they lead to divergent gas transfer velocities, particularly above 5 m s^{-1}, illustrated by a RMSE for SW as high as 22.8 cm h^{-1} for *CC98* while *CW03* performs better (RMSE SW = 12.8 cm h^{-1}). Furthermore, both models underestimate k_{600} at low wind (Fig. 4a), with a higher deviation for *CW03* (Table 2). The *k* values predicted by *VP13* are closer to those of the process-based models that explicitly integrate wave actions (*S07* and *DM18*) (Fig. 4bc), demonstrating that lake size integration in the empirical model captures at least part of the wave action on *k*. Performances of *VP13* at strong winds (RMSE SW = 12.7 cm h^{-1}) were better than those of the ocean-derived models integrating surface waves (RMSE SW = 13–15.9 cm h^{-1}). However, *VP13* shows a positive offset during calm periods, along with the highest RMSE of the set of models at low wind speed (Fig. 4b; Table 2).

Figure 4

The process-based models (Fig. 4c) provide different k_{600} values for a given wind speed, owing to the integration of additional environmental components (i.e., the varying drag coefficient, the convective mixing in *R12* and *T14* as well as the effect of waves in *S07*, *DM18*, *SD20* and *SD20-fit)*. All process-based models are similar at low winds as they share a common physical basis for parameterization of wind shear and convection. Therefore, they lead to similar RMSE (2.9–3.5 cm h^{-1}) under such conditions, where surface waves are negligible (Table 2). Divergences occur at higher wind speeds. *T14*, initially developed for small lakes with limited wind exposure, performed the worst (RMSE: 19.8 cm h^{-1}). This increased *k*-underestimation at high winds can be attributed to (i) dissipation by wave action and bubble formation not considered (in *R12* and *T14*), and (ii) to the use of a constant $z(0)$ = 0.15 m in the *T14* model (Eq. 5). This approximation of the diffusive layer is consistent with low wind speed but is almost one order of magnitude too large under strong wind speed. Other process-based models, designed for greater wind range (> 10 ms^{-1}), integrate surface waves and, as a result, lead to better estimates than *R12* and *T14* (RMSE: 10.4–15.9 cm h^{-1}). However, the ocean wave model of *DM18* shows lower performances at strong winds than *CW03* and *VP13*

https://doi.org/10.5194/esd-2021-30
Preprint. Discussion started: 7 May 2021


Earth System Dynamics Discussions

(Fig. 4bc). Finally, the specific fit parameterization of the *SD20-fit* model improves the performance at high wind speeds by ~30 % (RMSE = 10.5 cm h^{-1}), outperforming all the other methods.

Table 2

3.2 Surface wave integration

We herein scrutinize how those varying parameterizations ultimately alter the shape of relationship between k_{600} and U_{10}. In *R12* (Fig. 5a), wind is only included through wind shear, resulting in a linear relationship between k_{600} and U_{10}, as already anticipated. Adding the wave action (no bubble) through the *S07* parameterization (Fig. 5b) does not lead to any significant departure from the minimal *R12* model. Adapting wave action by decreasing C_T (for the no-bubble term) leads to a departure from the wind shear linear relationship for H_s > 0.4 m (Fig. 5c).

Then, adding the *k* bubble term related to wave breaking of *DM18* further increases this deviation from the linear k_{600}-U_{10} relationship but also scatters k_{600} estimates for a given U_{10} (Fig. 5d). Finally, the fitting with observationally based k_{600} improves the estimation for strong wind (Fig. 5e; Table 2). Given the range of wind fetch from ~ 0.5 km to ~30 km, the contribution of waves varies for a given wind speed depending on the fetch, as evidenced by the scattering of the parameterized k_{600} for a given U_{10} (Fig. 5f). A significant modification of k_{600} by wave action and wave breaking occurs for a fetch length > 15 km and U_{10} > 5 m s^{-1} (Fig. 5f), in the case of Lake Geneva, generating wave of H_s > 0.4 m (Fig. 5e).

Figure 5

As compared to k_{600} estimated by *R12* (Fig. 5a), the *SD20* and *SD20-fit* models provide *k* estimates that are 20–50 % higher for U_{10} = 10 m s^{-1}, respectively, and 40–70 % higher for U_{10} = 15 m s^{-1}. Therefore, adapting the surface waves, through the change of the wave action for incompletely developed waves and the fitting to observed data encountered in local lake conditions, leads to better performances of *SD20* models. *SD20-fit* reached the lowest RMSE at all wind speeds and is thereafter used as a reference for the modelling of the annual gas transfer velocities.

3.3 Annual cumulative gas transfer velocity and the effect of extreme conditions

We show above that models accounting for surface waves better represent the non-linear increase in k_{600} at high winds. Because high-wind events remain rare, we test whether a better representation of k_{600} during rare, high-wind events affects the local estimates of k_{600} over a full year. To this end, cumulative sums of hourly k_{600} were computed over a full annual cycle (13th June 2019 – 12th June 2020) for all *k*-models (Fig. 6). The annual dynamics such as the annually averaged k_{600} were compared using *SD20-fit* as a new reference model.

Figure 6

Cumulated k_{600} computed for *SD20-fit* shows some episodic steep increases between December and March, due to the winterly prevalence of high wind events (winter average wind speed, 3.25 m s^{-1}, was greater than the summer mean, 2.55 m s^{-1}, by 25 %) and greater significant wave height (winter average wave height, 0.15 m, greater than the summer value, 0.10 m, by 50 %)

https://doi.org/10.5194/esd-2021-30
Preprint. Discussion started: 7 May 2021


Earth System Dynamics Discussions

(Fig. C1). The average hourly k_{600} by the *SD20-fit* model is 7.3 ± 7.4 cm h^{-1} (mean ± se, Fig. 6a). Periods of high-winds, although accounting for 15 % of data points, contribute 44 % of annually cumulated-k_{600} in the *SD20* and *SD20-fit* models (Fig. 6b), while the periods of high waves ($H_s \geq 0.4$ m) accounting for only 6 % of data points, contribute to more than 20 % of annually cumulated-k_{600}.The wind-based models are those for which cumulative k_{600} diverges the most from the *SD20-fit* reference model, with the lowest annual averaged k_{600} for *CC98* and *CW03* (3.9 ± 2.7 and 4.8 ± 9.3 respectively) and the highest for *VP13* (9.9 ± 6.1). These divergences arise from the low performances of these models at low wind regimes (Fig. 4a, 6b; Table 2), which represent 85 % of annual data-points. All the other process-based models have relative dynamics of cumulative k_{600} similar to that of the *SD20-fit* model and end up with annually averaged k_{600} that are 15 % lower than for the *SD20-fit*. The representation of k_{600} at low wind speeds is similar for all process-based models, and the divergence arises from the representation of the rarer high wind speed episodes, which contribute to 43–46 % of annual cumulative k_{600} (Fig. 6b).

4 Discussion

The history of *k*-models, simulating the gas transfer velocity for surface waters, dates back from the early 1990's. *k*-models have been developed and tested in small lakes sheltered from winds (e.g., Crusius and Wanninkhof, 2003; Tedford et al., 2014), large lakes under low to moderate wind speed (Vachon and Prairie, 2013), and oceans (e.g., Soloviev et al., 2007; Fairall et al., 2011; Esters et al., 2017; Deike and Melville, 2018). While the effects of surface waves on *k* can be neglected in small lakes, we question herein whether this assumption holds for large lakes such as Lake Geneva, in which surface waves are frequently observed (Fig. 2; Fig. C1). We evaluated the performance of different experimental-based and process-based models to estimate k_{600} in the large Lake Geneva. We show that integrating the effect of wave formation at high wind speeds and long fetch better represents the sharp increase of the k_{600} values during such episodic windy events.

4.1 Choice of *k*-models

Wind-based models have been long known for misestimating k_{600} at low wind speeds (Eugster et al., 2003; MacIntyre et al., 2010; Erkkilä et al., 2018). Consistently, wind-based models showed the lowest performances for Lake Geneva, especially at low wind speeds (*CW03* and *VP13*), which resulted in large discrepancies in annually averaged and cumulative k_{600} over the full year. They are however easy to compute, require few inputs (only U_{10}) and, remain by far the most used to estimate lakes CO_2 emissions worldwide (e.g., Raymond et al. 2013). One solution to increase the performance of wind-based models is to revise calibration at each new site (Klaus and Vachon, 2020). Another possibility is to broadly adopt process-based models. The presented process-based models require input data that are today more easily accessible: wind speed, heat flux and wind fetch (i.e., distances from the shore) routinely acquired at high-frequency in many lakes. The development of R packages such as Lake Metabolizer (Winslow et al., 2016) in which the calculations of process-based models are implemented, also alleviates their computational difficulty. Both increased data availability and computational tools should foster the use of process-based *k*-models, which hold great potential to obtain more accurate global k_{600} estimates.

https://doi.org/10.5194/esd-2021-30
Preprint. Discussion started: 7 May 2021


Earth System Dynamics Discussions

The analysis of the models adapted from the existing literature to account for the effect of waves, *SD20* and *SD20-fit* (Fig. 5d-e-f), showed that the wave contribution to k becomes significant for H_s > 0.4 m, corresponding, for Lake Geneva, to winds blowing at 5 m s^{-1} from the southwest where the fetch length is maximal (> 15 km) with respect to the measurement site. A significant to the gas transfer velocity by surface waves is expected in lakes where H_s > 0.4 m is not infrequent. Wave heights beyond this threshold value of H_s are frequently encountered in lakes of similar or greater sizes than Lake Geneva (6 % of annual time in Lake Geneva). In the Great Lakes of North America, Hubertz et al. (1991) showed that the mean wave height of all these lakes were > 0.4 m in summer and close to 1 m in winter with a maximum of up to 5 m. H_s > 0.4 m can also form over elongated lakes of smaller size, such as smaller Swiss Lakes (e.g., Lake Neuchâtel, Lake Bienne) (Amini et al., 2017). Since *SD20-fit* is a process-based model integrating the four main processes in a mathematically coherent way, we would expect that it can be applied to such lakes experiencing H_s > 0.4 m and improves the accuracy of k estimates. Because waves can physically damage in-shore and off-shore infra-structures, many large lakes benefit from wave forecasts. H_s-data from those forecasting systems (e.g., National Data Buoy Centre – NOAA, Wave Atlas from SwissLakes.net; Amini et al., 2017) could allow testing whether the *SD20-fit* models can be applied to those lakes and whether k_{NB} and k_B through a_1 and A_b need to be recalibrated or fitted to the local context if flux measurement data are available, as for this study. Energy dissipation during high-wave events increases the gas-transfer velocity well beyond the linear relationship derived for wind shear alone. We therefore expect that computed gas fluxes at the air-water interface should be significantly improved by the integration of surface waves into the k-models.

4.2 Implication of four components on the annual k estimation and the annual CO_2 fluxes

4.2.1 Seasonal distribution of k_{CO2}

Converting k_{600} to k_{CO2} using the Schmidt number (Wanninkhof, 1992) highlights the importance of water temperature in gas exchange dynamics. Indeed, the seasonal distribution of the cumulative k_{600} is ~20 % and ~30 % for the warm (spring and summer) and cold (autumn and winter) seasons, respectively. Once the temperature-effect accounted for, this distribution increases to 26.1 % for the summer and decreases to 24.9 % for the winter but remains unchanged for spring and autumn. While *R12* only use wind shear and convective terms, the selected process-based model (*SD20-fit*) allows a decomposition into the four main drivers of the gas transfer velocity, hence paving the way to a better understanding of the implication of these processes throughout an annual cycle.

Figure 7

Wind shear remains the dominant component of the gas exchange velocity over the different seasons (Fig. 7a). The annual contribution of surface waves (wave action and bubble formation) is limited to 9 to 10 % of the cumulative k in Autumn and Winter. The contribution of buoyancy flux at surface to k is even smaller for both models (*R12* and *SD20-fit*) at this seasonal scale. Yet, both the buoyancy flux and the surface waves can significantly increase k during episodic events, during which

https://doi.org/10.5194/esd-2021-30
Preprint. Discussion started: 7 May 2021


Earth System Dynamics Discussions

they can contribute disproportionately to *k* at hourly (up to 80% for convection) and daily (up to 25 % for surface waves) time scales (Fig. 7b). Several studies have emphasized the disproportionate contribution of episodic mixing events on annual flux, bringing CO_2 back to lake surfaces such as after ice break in dimictic lakes (Karlsson et al., 2013; Finlay et al., 2019) or during fall mixing on a eutrophic deep lake (Reed et al., 2018). Process-based *k*-models integrating both the buoyancy flux and the wind-induced waves offer the opportunity to mechanistically investigate how much those episodic events contribute to annual emissions through short-term modifications of the gas exchange velocity.

4.2.2 Consequences on the choice of *k*-model on the monthly to annual CO_2 flux estimation

Monthly fluxes were computed based on *k*-estimates from the different models at hourly timestep and the monthly average of water temperature and recorded pCO_2 at the lake surface (OLA-IS, AnaEE-France, INRAE of Thonon-les-Bains, CIPEL, Rimet et al., 2020; Perga et al., 2016) as well as a constant pCO_2 in the atmosphere (400 µatm). As predicted by the Fick's law, the highest outgassing fluxes occur in fall and winter, when water mixing brings CO_2 up to the lake surface, while low up-taking gas fluxes occur in spring and summer, when primary production depletes surface CO_2 below saturation. However, annual estimates of net CO_2 outgassing vary from 14.7 to 37.1 mmolC m^{-2} d^{-1} (Table 3) depending on the *k*-model used for computation. Consistently, differences between model estimates are relatively low in summer since both the ΔpCO_2 gradient (100-200 µatm) and wave occurrence are limited. Estimated fluxes are strongly dependent on the chosen *k*-model in winter when both ΔpCO_2 (475 µatm) and surface waves occurrence are higher (Table 3; Fig.7). Therefore, while high wave events represent only 6 % of the total surface waves occurrence (H_s > 0.4 m), an incomplete consideration and description of their contribution may lead to an annual flux underestimation of about 20–25 %. The weak contribution of convection is at odds with observations in small lakes, but not unexpected, since large lakes are exposed to stronger winds, such that wind shear-driven ε_u often outpaces convectively driven, ε_c (Read et al, 2012). However, the limited impact of the buoyancy flux on *k* does not rule out its contribution to CO_2 exchange. Indeed, convective mixing plays a central role in the deepening of the mixed layer allowing the export of the CO_2 stored in the hypolimnion towards the surface during the cold period and thereby controlling the pCO_2 gradient (Zimmerman et al, 2020) and the observed wintertime outgassing. Altogether, both surface oversaturated CO_2 concentrations (as a result of convective mixing) and wind-induced waves are more relevant in fall and wintertime for the monomictic Lake Geneva, leading to most of the annual outgassing during this season (Table 3). As for many monomictic lakes, these seasons drive most of the annual CO_2 budget of Lake Geneva (Perga et al, 2016), while they usually correspond to those where direct measurements are the scarcest. An improved quantification of *k*-values through SRM-models including wind-induced waves should contribute to refining the overall estimation of large lakes contribution to regional CO_2 emissions.

Table 3

https://doi.org/10.5194/esd-2021-30
Preprint. Discussion started: 7 May 2021


Earth System Dynamics Discussions Open Access EGU

5 Conclusion

Investigations of the four main processes generating the gas transfer velocity in the large Lake Geneva demonstrated the importance of considering surface waves during episodic windy events responsible for more than 44 % of annual cumulated k_{600}. The in-depth study of the behaviour of the process-based models has enabled to underscore their consistent predictions at low and strong wind, especially considering the new combination and adaptation model, *SD20-fit*. This last model significantly improves the estimation of CO_2 flux when these three thresholds appear in the field: $U_{10} > 5$ ms^{-1}, Fetch > 15 km, and $H_s > 0.4$ m, making it applicable in a wide range of lake sizes. Furthermore, *SD20-fit* is assembled on solid theoretical bases coming from limnological and oceanic literature and allows to analyse the distribution of these four main terms (k_u, k_c, k_w, and k_b) across a variety of time scales depending on the kind of study.

Noteworthily, *SD20* was built on the basis of a single measurement point on the lake, just as for most of the existing *k* models. Therefore, the question of the extrapolation of the model to the whole of the lake remains essential. We assume three ways of different complexities: (i) estimate an average fetch value depending on the wind direction and the geometry of the lake, (ii) discretize the lake into a few parts according to the complexity of its geometry and direction of the prevailing winds, and (iii) discretize the lake into a large number of pixels based on 2D or 3D wind models available in some countries in order to estimate gas transfer velocity and gas fluxes at a finer spatial scale. Nevertheless, the question of the spatial variability of the ΔCO_2 is still open and difficult to analyse at high frequency in large lakes.

To conclude, this study sheds light on the complexity of large lakes located at the interface between small, sheltered lakes and the open oceans, thus experiencing a combination of processes relevant for both small and large systems. The possibility of using process-based models in a fairly simple way with few inputs to improve the precision of the gas transfer velocity and therefore the gas flux should be supported in future research. In addition, this approach is very promising regarding long-term trends of CO_2 emissions from lakes, as well as a finer estimation of fluxes during more intense episodic events.

Appendix A

Figure A1

Figure A2

Figure A3

Appendix B

Figure B1

https://doi.org/10.5194/esd-2021-30
Preprint. Discussion started: 7 May 2021

Appendix C

Figure C1

Data availability. Water temperature, buoyancy flux at surface, and meteorological data are available in the datalakes – Open research data publishing platform (https://www.datalakes-eawag.ch). Water CO_2 concentration and CO_2 flux measurements are available upon request from the first author.

Author contribution. PP, MEP, and DB designed the study. PP, BFC, NE, and TL collected field data and carried out data pre-processing. PP developed the model code and performed the simulation with contribution from DB. PP, MEP, and DB drafted the manuscript and all co-authors contributed to the final submitted manuscript.

Competing interests. The authors declare that they have no conflict of interest.

Acknowledgements. We would like to thank the entire team from LéXPLORE platform, for their administrative and technical support and for LéXPLORE core dataset. We also acknowledge LéXPLORE five partner institutions: Eawag, EPFL, University of Geneva, University of Lausanne and CARRTEL (INRAE-USMB). This study was supported by CARBOGEN project (SNF 200021_175530) linked to LéXPLORE project (SNF R'Equip, P157779). The authors thanks Sébastien Lavanchy, chief technical officer (APHYS-EPFL) and Aurélien Ballu, member of the technical pool (IDYST-UNIL) of LéXPLORE platform for their technical and field supports. B. F. C. was supported by the European Union's Horizon 2020 research and innovation program under the Marie Skłodowska-Curie grant agreement No. 834330 (SO-CUP).

References

Amini, A., Dhont, B., and Heller, P.: Wave atlas for Swiss lakes: modeling design waves in mountainous lakes, J. Appl. Wat. Eng. Res., 5, 103–113, https://doi.org/10.1080/23249676.2016.1171733, 2017.

Bastviken, D., Sundgren, I., Natchimuthu, S., Reyier, H. and Gålfalk, M.: Technical Note: Cost-efficient approaches to measure carbon dioxide (CO_2) fluxes and concentrations in terrestrial and aquatic environments using mini loggers, Biogeosciences, 12, 3849–3859, https://doi.org/10.5194/bg-12-3849-2015, 2015.

Borges, A. V., Vanderborght, J.-P., Schiettecatte, L.-S., Gazeau, F., Ferron-Smith, S., Delille, B. and Frankignoulle, M.: Variability of the gas transfer velocity of CO_2 in a macrotidal estuary (the Scheldt), Estuaries, 27, 593–603, https://doi.org/10.1007/BF02907647, 2004.

Carter, D. J. T.: Prediction of wave height and period for a constant wind velocity using the JONSWAP results. Ocean Eng., 9, 17–33, https://doi.org/10.1016/0029-8018(82)90042-7, 1982.

https://doi.org/10.5194/esd-2021-30
Preprint. Discussion started: 7 May 2021


Earth System Dynamics Discussions

Cole, J. J., Bade, D. L., Bastviken, D., Pace, M. L., & de Bogert, M. V.: Multiple approaches to estimating air-water gas exchange in small lakes, Limnol. Oceanogr.: Methods, 8, https//doi.org/10.4319/lom.2010.8.285, 2010.

Cole, J. J., Prairie, Y. T., Caraco, N. F., McDowell, W. H., Tranvik, L. J., Striegl, R. G., Duarte, C. M., Kortelainen, P., Downing, J. A., Middelburg, J. J. and Melack, J.: Plumbing the Global carbon cycle: Integrating inland waters into the terrestrial carbon budget, Ecosystems, 10, 172–185, https://doi.org/10.1007/s10021-006-9013-8, 2007.

Cole, J. J. and Caraco, N. F.: Atmospheric exchange of carbon dioxide in a low-wind oligotrophic lake measured by the addition of SF_6, Limnol. Oceanogr., 43, 647–656, https://doi.org/10.4319/lo.1998.43.4.0647, 1998.

Crusius, J. and Wanninkhof, R.: Gas transfer velocities measured at low wind speed over a lake, Limnol. Oceanogr., 48, 1010–1017, https://doi.org/10.4319/lo.2003.48.3.1010, 2003.

Danckwerts, P. V.: Significance of liquid-film coefficient in gas absorption, Ind. Eng. Chem., 43, 1460–1467, https://doi.org/10.1021/ie50498a055, 1951.

Deike, L. and Melville, W. K.: Gas transfer by breaking waves, Geophys. Res. Lett., 45, 482–492, https://doi.org/10.1029/2018GL078758, 2018.

Dugan, H. A., Woolway, R. I., Santoso, A. B., Corman, J. R., Jaimes, A., Nodine, E. R., Patil, V. P., Zwart, J. A., Brentrup, J. A., Hetherington, A. L., Oliver, S. K., Read, J. S., Winters, K. M., Hanson, P. C., Read, E. K., Winslow, L. A. and Weathers, K. C.: Consequences of gas flux model choice on the interpretation of metabolic balance across 15 lakes, Inland Waters, 6, 581–592, https://doi.org/10.1080/IW-6.4.836, 2016.

Engel, F., Farrell, K. J., McCullough, I. M., Scordo, F., Denfeld, B. A., Dugan, H. A., de Eyto, E., Hanson, P. C., McClure, R. P., Nõges, P., Nõges, T., Ryder, E., Weathers, K. C. and Weyhenmeyer, G. A.: A lake classification concept for a more accurate global estimate of the dissolved inorganic carbon export from terrestrial ecosystems to inland waters, The Science of Nature, 105, https://doi.org/10.1007/s00114-018-1547-z, 2018.

Erkkilä, K.-M., Ojala, A., Bastviken, D., Biermann, T., Heiskanen, J. J., Lindroth, A., Peltola, O., Rantakari, M., Vesala, T. and Mammarella, I.: Methane and carbon dioxide fluxes over a lake: comparison between eddy covariance, floating chambers, and boundary layer method, Biogeosciences, 15, 429–445, https://doi.org/10.5194/bg-15-429-2018, 2018.

Esters, L., Landwehr, S., Sutherland, G., Bell, T. G., Christensen, K. H., Saltzman, E. S., Miller, S. D., & Ward, B.: Parameterizing air-sea gas transfer velocity with dissipation: Dissipation-based k-parametrization. J. Geophys. Res.-Oceans, 122, 3041–3056. https://doi.org/10.1002/2016JC012088, 2017.

Eugster, W., Kling, G. W., Jonas, T., McFadden, J. P., Wüest, A., MacIntyre, S. and Chapin, F. S.: CO_2 exchange between air and water in an Artic Alaskan and midlatitude Swiss lake: Importance of convective mixing, J. Geophys. Res., 108, https://doi.org/10.1029/2002JD002653, 2003.

Fairall, C. W., Yang, M., Bariteau, L., Edson, J. B., Helmig, D., McGillis, W., Pezoa, S., Hare, J. E., Huebert, B. and Blomquist, B.: Implementation of the Coupled Ocean-Atmosphere Response Experiment flux algorithm with CO_2, dimethyl sulfide, and O_3, J. Geophys. Res., 116, https://doi.org/10.1029/2010JC006884, 2011.

Finlay, K., Vogt, R. J., Simpson, G. L. and Leavitt, P. R.: Seasonality of pCO_2 in a hard-water lake of the northern Great

Plains: The legacy effects of climate and limnological conditions over 36 years, Limnol. Oceanogr., 64, 118–129, https://doi.org/10.1002/lno.11113, 2019.

Frost, T. and Upstill-Goddard, R. C.: Meteorological controls of gas exchange at a small English lake, Limnol. Oceanogr., 47, 1165–1174, https://doi.org/10.4319/lo.2002.47.4.1165, 2002.

Guérin, F., Abril, G., Serça, D., Delon, C., Richard, S., Delmas, R., Tremblay, A. and Varfalvy, L.: Gas transfer velocities of CO_2 and CH_4 in a tropical reservoir and its river downstream, J. Marine Syst., 66, 161–172, https://doi.org/10.1016/j.jmarsys.2006.03.019, 2007.

Hasselmann K., Barnett T.P., Bouws, E., Carlson, H, Cartwright D.E., et al.: Measurements of wind-wave growth and swell decay during the Joint North Sea Wave Project (JON- SWAP), Dtsch. Hydrog. Z. Suppl. A, 8, 95 pp., 1973.

Heiskanen, J. J., Mammarella, I., Haapanala, S., Pumpanen, J., Vesala, T., MacIntyre, S. and Ojala, A.: Effects of cooling and internal wave motions on gas transfer coefficients in a boreal lake, Tellus B, 66, https://doi.org/10.3402/tellusb.v66.22827, 2014.

Hubertz, J. M., Driver, D. B., and Reinhard, R. D.: Wind waves on the Great Lakes: A 32 year hindcast. J. Coastal Res., 7, 945–967. ISSN 0749-02208, 1991.

Huotari, J., Ojala, A., Peltomaa, E., Nordbo, A., Launiainen, S., Pumpanen, J., Rasilo, T., Hari, P. and Vesala, T.: Long-term direct CO_2 flux measurements over a boreal lake: Five years of eddy covariance data, Geophys. Res. Lett., 38, https://doi.org/10.1029/2011GL048753, 2011.

Karlsson, J., Giesler, R., Persson, J. and Lundin, E.: High emission of carbon dioxide and methane during ice thaw in high latitude lakes, Geophys. Res. Lett., 40, 1123–1127, https://doi.org/10.1002/grl.50152, 2013.

Katul, G. and Liu, H.: Multiple mechanisms generate a universal scaling with dissipation for the air-water gas transfer velocity, Geophys. Res. Lett., 44, 1892–1898, https://doi.org/10.1002/2016GL072256, 2017.

Katul, G., Mammarella, I., Grönholm, T. and Vesala, T.: A structure function model recovers the many formulations for air-water gas transfer velocity, Water Resour. Res., 54, 5905–5920, https://doi.org/10.1029/2018WR022731, 2018.

Keeling, R. F., Najjar, R. P., Bender, M. L. and Tans, P. P.: What atmospheric oxygen measurements can tell us about the global carbon cycle, Global Biogeochem. Cycles, 7(1), 37–67, https://doi.org/10.1029/92GB02733, 1993.

Klaus, M. and Vachon, D.: Challenges of predicting gas transfer velocity from wind measurements over global lakes, Aquat. Sci., 82, https://doi.org/10.1007/s00027-020-00729-9, 2020.

Lamont, J. C. and Scott, D. S.: An eddy cell model of mass transfer into the surface of a turbulent liquid, AIChE J., 16, 513–519, https://doi.org/10.1002/aic.690160403, 1970.

Lombardo, C. P., & Gregg, M. C.: Similarity scaling of viscous and thermal dissipation in a convecting surface boundary layer. J. Geophys. Res., 94, 6273–6284, https://doi.org/10.1029/jc094ic05p06273, 1989.

Lorke, A. and Peeters, F.: Toward a unified scaling relation for interfacial fluxes, J. Phys. Oceanogr., 36, 955–961, https://doi.org/10.1175/JPO2903.1, 2006.

Maberly, S. C., Barker, P. A., Stott, A. W. and De Ville, M. M.: Catchment productivity controls CO_2 emissions from lakes,

Nat. Clim. Change, 3, 391–394, https://doi.org/10.1038/nclimate1748, 2013.

MacIntyre, S., Jonsson, A., Jansson, M., Aberg, J., Turney, D. E. and Miller, S. D.: Buoyancy flux, turbulence, and the gas transfer coefficient in a stratified lake: Turbulence and gas evasion in lakes, Geophys. Res. Lett., 37, L24604, https://doi.org/10.1029/2010GL044164, 2010.

MacIntyre, S., Eugster, W. and Kling, G. W.: The critical importance of buoyancy flux for gas flux across the air-water interface, in Geophysical Monograph Series, edited by M. A. Donelan, W. M. Drennan, E. S. Saltzman, and R. Wanninkhof, pp. 135–139, American Geophysical Union, Washington, D. C., https://doi.org/10.1029/GM127p0135, 2001.

Mammarella, I., Nordbo, A., Rannik, Ü., Haapanala, S., Levula, J., Laakso, H., Ojala, A., Peltola, O., Heiskanen, J., Pumpanen, J. and Vesala, T.: Carbon dioxide and energy fluxes over a small boreal lake in Southern Finland: CO_2 and Energy Fluxes Over Lake, J. Geophys. Res. Biogeosci., 120, 1296–1314, https://doi.org/10.1002/2014JG002873, 2015.

Perga, M.-E., Maberly, S. C., Jenny, J.-P., Alric, B., Pignol, C. and Naffrechoux, E.: A century of human-driven changes in the carbon dioxide concentration of lakes: 150 years of human impacts on lakes CO_2, Global Biogeochem. Cy., 30, 93–104, https://doi.org/10.1002/2015GB005286, 2016.

Raymond, P. A., Hartmann, J., Lauerwald, R., Sobek, S., McDonald, C., Hoover, M., Butman, D., Striegl, R., Mayorga, E., Humborg, C., Kortelainen, P., Dürr, H., Meybeck, M., Ciais, P. and Guth, P.: Global carbon dioxide emissions from inland waters, Nature, 503, 355–359, https://doi.org/10.1038/nature12760, 2013.

Read, J. S., Hamilton, D. P., Desai, A. R., Rose, K. C., MacIntyre, S., Lenters, J. D., Smyth, R. L., Hanson, P. C., Cole, J. J., Staehr, P. A., Rusak, J. A., Pierson, D. C., Brookes, J. D., Laas, A. and Wu, C. H.: Lake-size dependency of wind shear and convection as controls on gas exchange: Lake-size dependency of u_* and w_*, Geophys. Res. Lett., 39, L09405, https://doi.org/10.1029/2012GL051886, 2012.

Reed, D. E., Dugan, H. A., Flannery, A. L. and Desai, A. R.: Carbon sink and source dynamics of a eutrophic deep lake using multiple flux observations over multiple years: Carbon sink and source dynamics, Limnol. Oceanogr. Lett., 3, 285–292, https://doi.org/10.1002/lol2.10075, 2018.

Reichl, B. G. and Deike, L.: Contribution of sea-state dependent bubbles to air-sea carbon dioxide fluxes, Geophys. Res. Lett., 47, L087267, https://doi.org/10.1029/2020GL087267, 2020.

Rimet, F., Anneville, O., Barbet, D., Chardon, C., Crépin, L., Domaizon, I., Monet, G.: The Observatory on LAkes (OLA) database: Sixty years of environmental data accessible to the public. J. Limnol., 78, 164–178. doi:114810.4081/jlimnol.2020.1944, 2020.

Risk, D., Nickerson, N., Creelman, C., McArthur, G. and Owens, J.: Forced Diffusion soil flux: A new technique for continuous monitoring of soil gas efflux, Agr. Forest Meteorol., 151, 1622–1631, https://doi.org/10.1016/j.agrformet.2011.06.020, 2011.

Russell, T. W. F. and Denn, M. M.: Introduction to chemical engineering analysis, Wiley., 1972.

Schilder, J., Bastviken, D., van Hardenbroek, M., Kankaala, P., Rinta, P., Stötter, T. and Heiri, O.: Spatial heterogeneity and lake morphology affect diffusive greenhouse gas emission estimates of lakes: Spatial heterogeneity of diffusive flux, Geophys. Res. Lett., 40, 5752–5756, https://doi.org/10.1002/2013GL057669, 2013.

https://doi.org/10.5194/esd-2021-30
Preprint. Discussion started: 7 May 2021


Earth System Dynamics Discussions

Schubert, M., Paschke, A., Lieberman, E. and Burnett, W. C.: Air–Water Partitioning of ^{222}Rn and its Dependence on Water Temperature and Salinity, Environ. Sci. Technol., 46, 3905–3911, https://doi.org/10.1021/es204680n, 2012.

Simon, A.: Turbulent mixing in the surface boundary layer of lakes, Doctoral dissertation submitted to the Swiss Federal Institute of Technology Zurich, 1997.

Soloviev, A., Donelan, M., Graber, H., Haus, B. and Schlüssel, P.: An approach to estimation of near-surface turbulence and CO_2 transfer velocity from remote sensing data, Journal of Marine Systems, 66, 182–194, https://doi.org/10.1016/j.jmarsys.2006.03.023, 2007.

Soloviev, A., Lukas, R., 2006. The Near-Surface Layer of the Ocean: Structure, Dynamics, and Applications, Springer, 572 pp., https//doi.org/10.1007/978-94-007-7621-0, 2006.

Soloviev, A. and Schlüssel P.: Parametrization of the cool skin of the ocean and of the air-ocean gas transfer on the basis of modeling surface renewal, J. Phys. Oceanogr., 24, 1339–1346, 1994.

Stumm, W. and Morgan, J. J.: Aquatic Chemistry: An introduction emphasizing chemical equilibria in natural waters, 2nd Edition., 1981.

Tedford, E. W., MacIntyre, S., Miller, S. D. and Czikowsky, M. J.: Similarity scaling of turbulence in a temperate lake during fall cooling, J. Geophys. Res.-Oceans, 119, 4689–4713, https://doi.org/10.1002/2014JC010135, 2014.

Terray, E. A., Donelan, M. A., Agrawal, Y. C., Drennan, W. M., Kahma, K. K., Williams III, A. J., Hwang, P. A. and Kitaigorodkii, S. A.: Estimates of kinetic energy dissipation under breaking waves, J. Phys. Oceanogr., 26, 792–807, 1996.

Toba, Y.: Stochastic form of the growth of wind waves in a single-parameter representation with physical implications, J. of Physical Oceanography, 8, 494–507, https://doi.org/10.1175/1520-0485(1978)008<0494:SFOTGO>2.0.CO;2, 1978.

Toba, Y.: Local balance in the air-sea boundary processes, J. Oceanogr., 28, 109–120, https://doi.org/10.1007/BF02109772, 1972.

Tranvik, L. J., Downing, J. A., Cotner, J. B., Loiselle, S. A., Striegl, R. G., Ballatore, T. J., Dillon, P., Finlay, K., Fortino, K., Knoll, L. B., Kortelainen, P. L., Kutser, T., Larsen, Soren., Laurion, I., Leech, D. M., McCallister, S. L., McKnight, D. M., Melack, J. M., Overholt, E., Porter, J. A., Prairie, Y., Renwick, W. H., Roland, F., Sherman, B. S., Schindler, D. W., Sobek, S., Tremblay, A., Vanni, M. J., Verschoor, A. M., von Wachenfeldt, E. and Weyhenmeyer, G. A.: Lakes and reservoirs as regulators of carbon cycling and climate, Limnol. Oceanogr., 54, 2298–2314, https://doi.org/10.4319/lo.2009.54.6_part_2.2298, 2009.

Vachon, D. and Prairie, Y. T.: The ecosystem size and shape dependence of gas transfer velocity versus wind speed relationships in lakes, Can. J. Fish. Aquat. Sci., 70, 1757–1764, https://doi.org/10.1139/cjfas-2013-0241, 2013.

Vachon, D., Prairie, Y. T. and Cole, J. J.: The relationship between near-surface turbulence and gas transfer velocity in freshwater systems and its implications for floating chamber measurements of gas exchange, Limnol. Oceanogr., 55, 1723–1732, https://doi.org/10.4319/lo.2010.55.4.1723, 2010.

Vesala, T., Huotari, J., Rannik, Ü., Suni, T., Smolander, S., Sogachev, A., Launiainen, S. and Ojala, A.: Eddy covariance measurements of carbon exchange and latent and sensible heat fluxes over a boreal lake for a full open-water period, J.

Geophys. Res., 111, D11101, https://doi.org/10.1029/2005JD006365, 2006.

Wanninkhof, R.: Relationship between wind speed and gas exchange over the ocean, J. Geophys. Res., 97, 7373–7382, https://doi.org/10.1029/92JC00188, 1992.

Winslow, L. A., Zwart, J. A., Batt, R. D., Dugan, H. A., Woolway, R. I., Corman, J. R., Hanson, P. C., & Read, J. S.: LakeMetabolizer: An R package for estimating lake metabolism from free-water oxygen using diverse statistical models, Inland Waters, 6, 622–636. https://doi.org/10.1080/IW-6.4.883, 2016.

Wyngaard, J. C. and Coté O.R.: The budgets of turbulent kinetic energy and temperature variance in the atmospheric surface layer, J. Atmos. Sci., 28, 190–201, 1971.

Woolf, D. K.: Parametrization of gas transfer velocities and sea-state-dependent wave breaking, Tellus B, 57, 87–94, https://doi.org/10.3402/tellusb.v57i2.16783, 2005.

Woolf, D. K.: Bubbles and their role in gas exchange, in The Sea Surface and Global Change, edited by P. S. Liss and R. A. Duce, pp. 173–206, Cambridge University Press, https://doi.org/10.1017/CBO9780511525025.007, 1997.

Wüest, A. and Lorke, A.: Small-scale hydrodynamics in lakes, Annu. Rev. Fluid Mech., 35, 373–412, https://doi.org/10.1146/annurev.fluid.35.101101.161220, 2003.

Zappa, C. J., McGillis, W. R., Raymond, P. A., Edson, J. B., Hintsa, E. J., Zemmelink, H. J., Dacey, J. W. H. and Ho, D. T.: Environmental turbulent mixing controls on air-water gas exchange in marine and aquatic systems, Geophys. Res. Lett., 34, L10601, https://doi.org/10.1029/2006GL028790, 2007.

Zimmermann, M., Mayr, M. J., Bouffard, D., Eugster, W., Steinsberger, T., Wehrli, B., Brand, A., Bürgmann, H.: Lake overturn as a key driver for methan oxidation, CSH. Lab. bioRXiv, https://doi.org/10.1101/689182, 2019.

https://doi.org/10.5194/esd-2021-30
Preprint. Discussion started: 7 May 2021

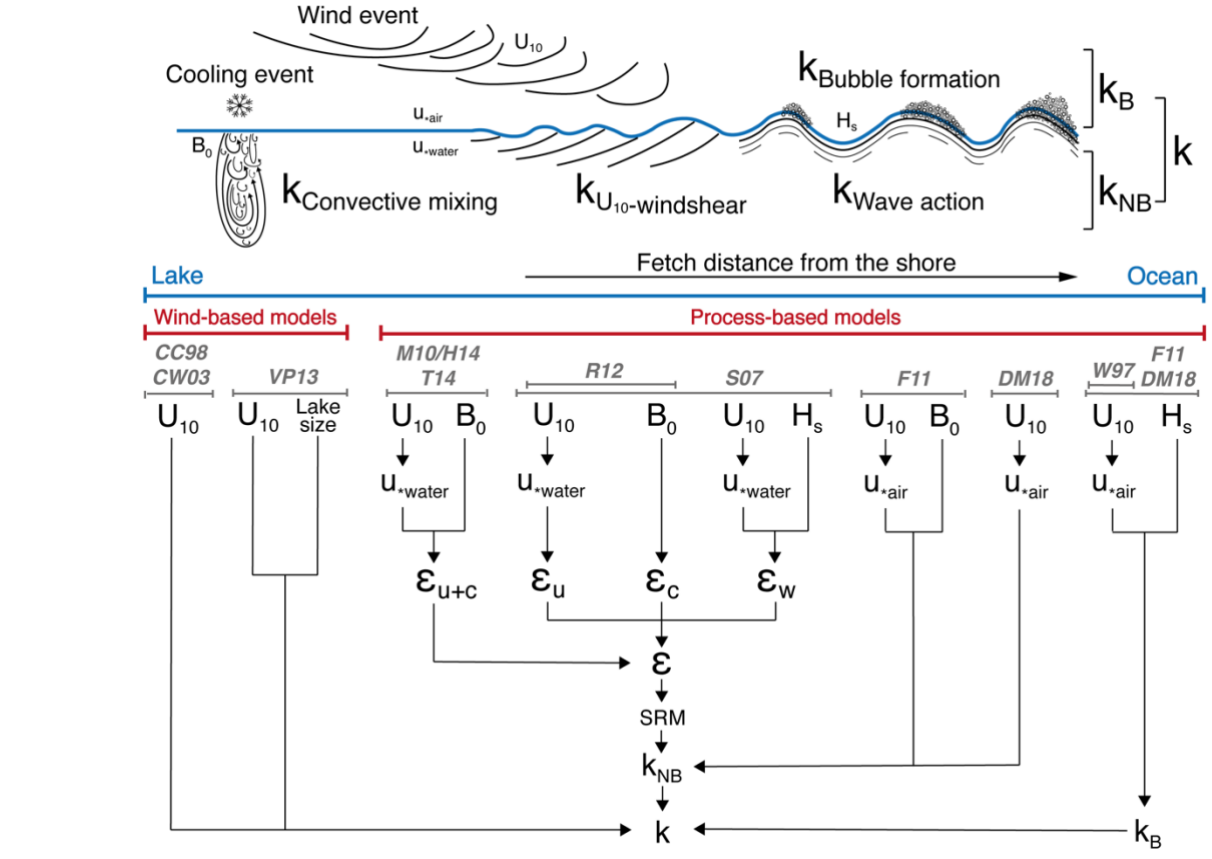

Figure 1: Conceptual scheme of the four main processes driving gas transfer velocity (*k*) in a large lake induced by wind and cooling events. These four processes are split into two types of *k*: *k*-bubble for the bubble formation ($k_B = k_b$) and *k*-no bubble for the convective mixing, wind shear and wave action term which are added ($k_{NB} = k_c + k_u + k_w$). Below this scheme, a non-exhaustive review about conceptual approaches of k-models used in 1st Fickian law. From left to right, increase in the complexity level of *k*-models as well as their study site (limnological to oceanic case). All these variables are described in the section 2.4 and in Table 1.

https://doi.org/10.5194/esd-2021-30
Preprint. Discussion started: 7 May 2021

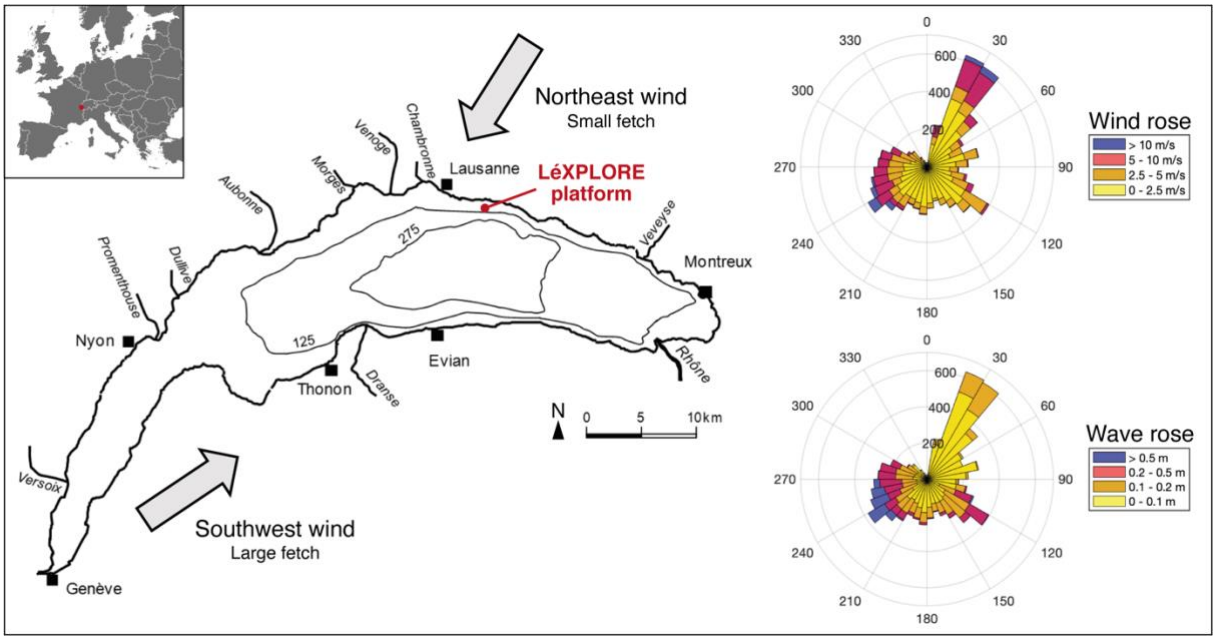

Figure 2: Location and map of Lake Geneva with the two prevailing winds (left side) also depicted by the wind rose (top right side). The wave rose highlights the highest wavefield generated at the sampling location by the southwest wind with a larger fetch (bottom right side). Both wind and wave roses are computed with annual data from 13th June 2019 to 12th June 2020 at LéXPLORE.

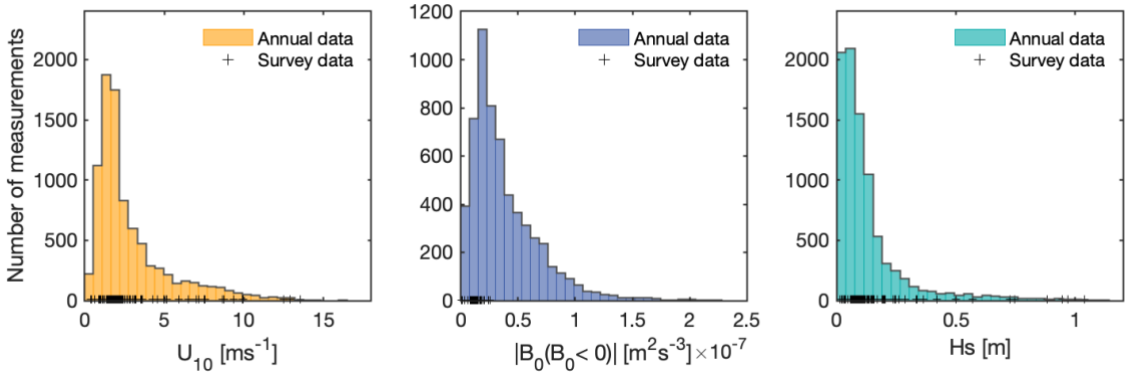

Figure 3: Annual distribution of three main components used to compute k_{600} models. Orange) Wind speed at 10 m; Blue) Buoyancy flux at surface during cooling; Turquoise) Significant wave height; and these survey data observed during CO_2 flux measurements after quality control (+).

https://doi.org/10.5194/esd-2021-30
Preprint. Discussion started: 7 May 2021

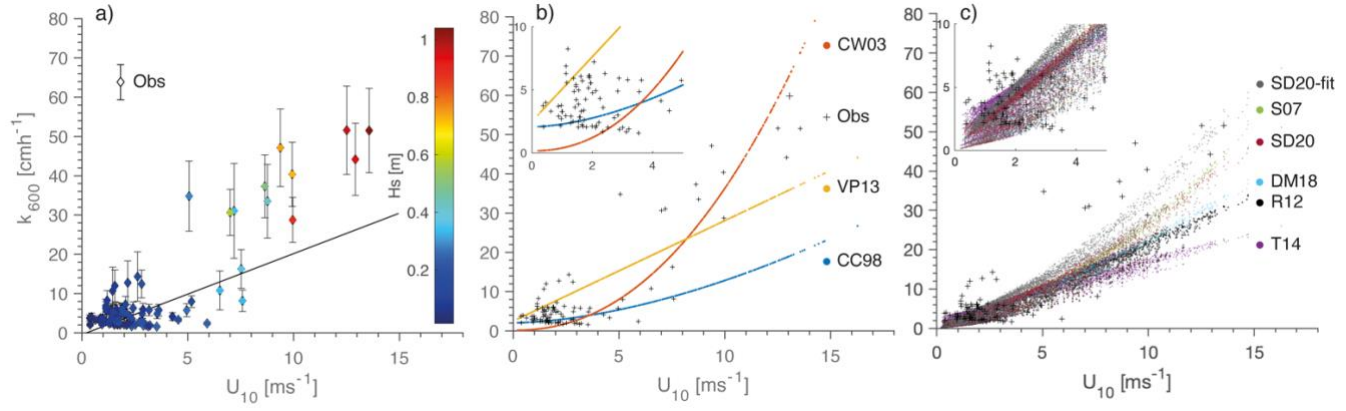

Figure 4: a) k_{600} observed as a function of U_{10} and coloured according to H_s (colorbar), and the error bars produced by the uncertainty of ΔCO_2 ($\pm$ 50 ppm) as well as the u_*-k_{600} linear regression (solid line: see also Fig. B1); b) k_{600} wind-based models (*CC98*, *CW03* & *VP13*); c) k_{600} process-based models (*T14*, *S07*, *DM18*, *SD20* & *SD20-fit*) computed with annual data; Observed k_{600} derived from CO_2 flux chamber measurements (+).

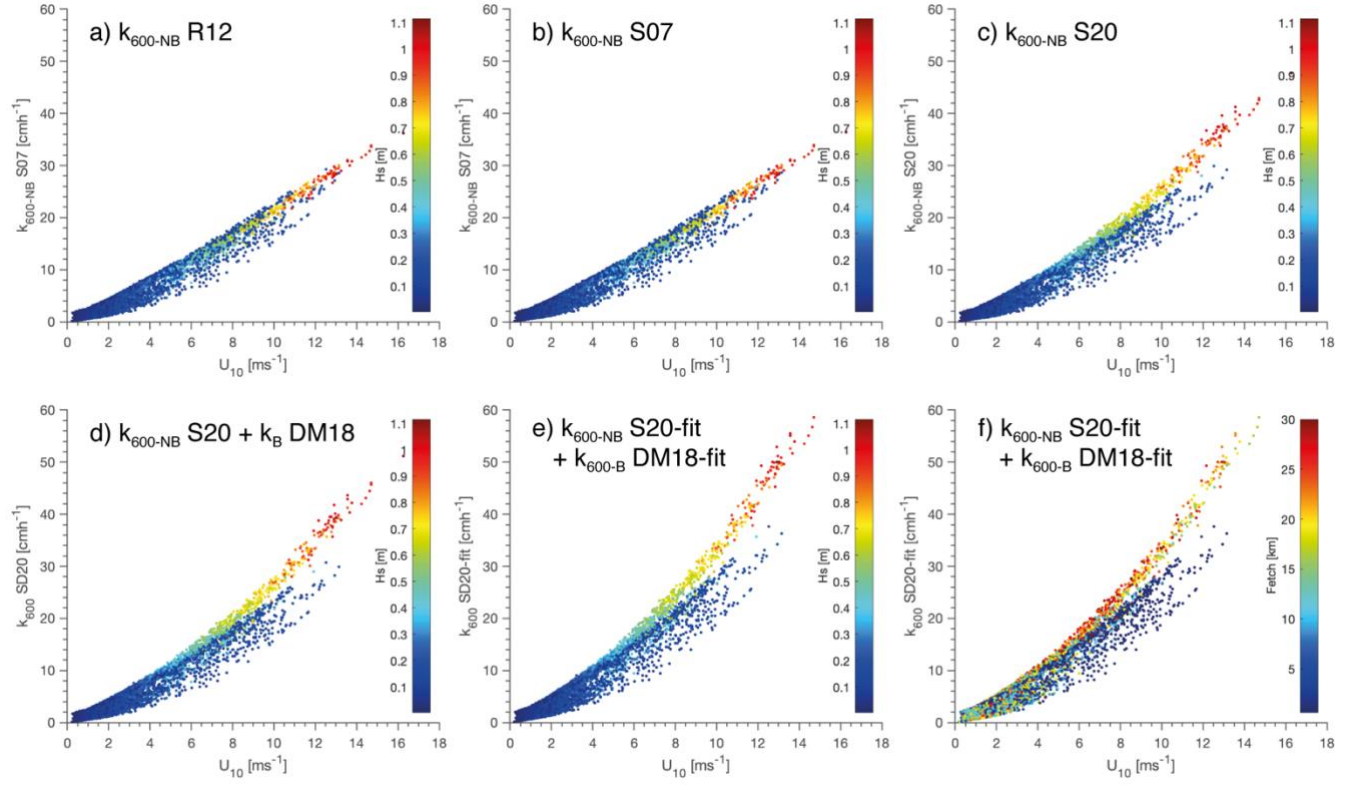

Figure 5: Relation U_{10} vs k_{600} modelled and coloured according to H_s (colorbar) in a-b-c-d-e as well as coloured according to fetch distance (colorbar) in f. a) *R12* integrating wind shear and convection; b) *S07* integrating wind shear, convection, and wave action for fully developed waves; c) *S20* integrating wind shear, convection, and wave action for not fully developed waves; d) *SD20* similar to *S20* adding the *k* bubble term of *DM18*; e-f) *SD20-fit* similar to *SD20* with a_1 and A_b fitted to *k* observed.

https://doi.org/10.5194/esd-2021-30
Preprint. Discussion started: 7 May 2021

Earth System Dynamics
Discussions
Open Access
EGU

675

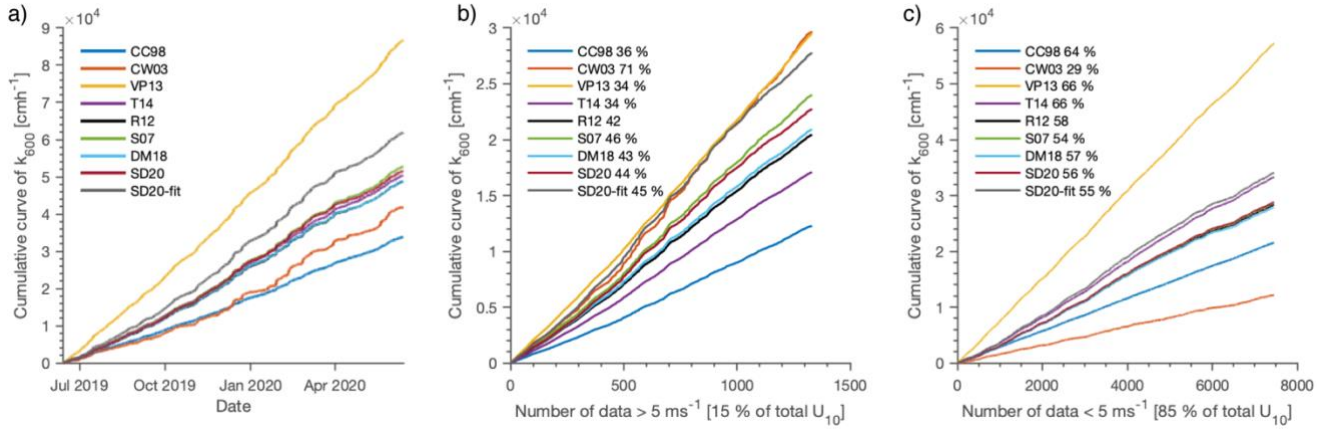

Figure 6: a) Cumulative k_{600} modelled over an annual cycle; b) Cumulative k_{600} for wind < 5 m s^{-1}; c) Cumulative k_{600} for wind ≥ 5 m s^{-1}.

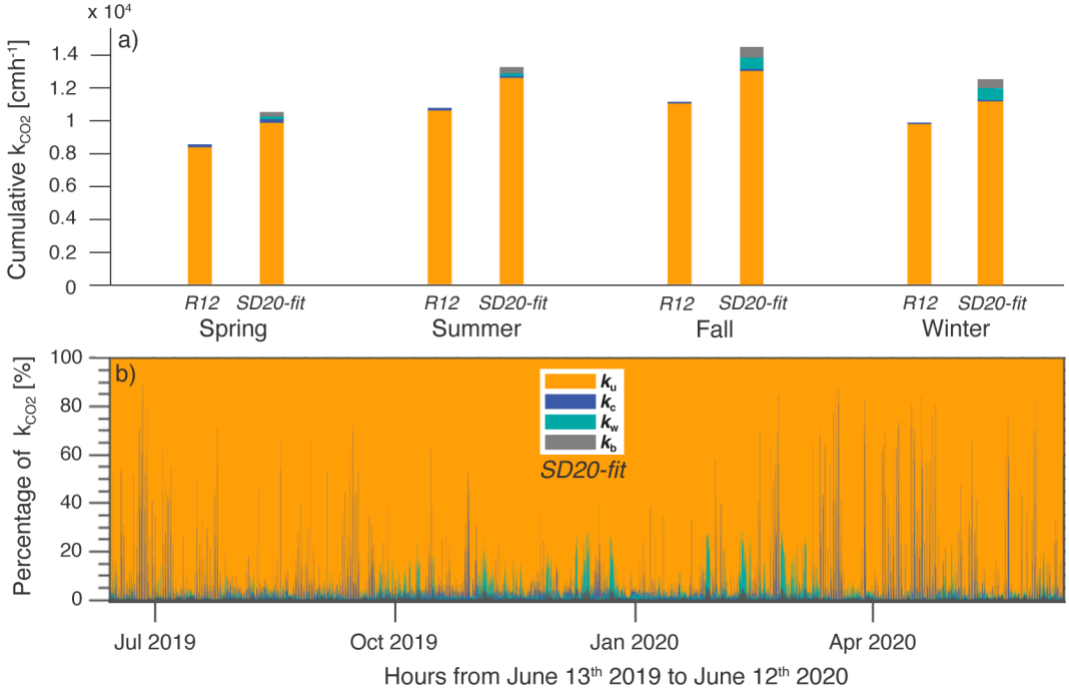

680 **Figure 7: a) Distribution of k_{CO2} generated by two main processes (k_u and k_c) in *R12* and four main processes (k_u, k_c, k_w, and k_b) in *SD20-fit* for each season; Spring (April-May-June); Summer (July-August-September); Fall (October-November-December); Winter (January-February-March). The height of bar represents the cumulative of k_{CO2} by season for both models (*R12* and *SD20-fit*); b) Distribution of four *k* generated by wind shear, convection, wave action and bubble enhancement (k_u, k_c, k_w, and k_b) along the annual cycle. Use of *SD20-fit* model where $k_u = SRM(\varepsilon_u)$, $k_c =$**
685 **$SRM(\varepsilon_u + \varepsilon_c + \varepsilon_w) - SRM(\varepsilon_u + \varepsilon_w)$, $k_w = SRM(\varepsilon_u + \varepsilon_c + \varepsilon_w) - SRM(\varepsilon_u + \varepsilon_c)$, and k_b.**

https://doi.org/10.5194/esd-2021-30
Preprint. Discussion started: 7 May 2021

Earth System Dynamics Discussions

Table 1: Summary of characteristics of k_{Sc} models for predicting the air-water gas transfer velocity based on wind speed (*CC98, CW03*) and lake size (*VP13*), surface renewal model (*T14, R12* & *S07*), COARSE approach (*DM18*) and both adapted models called *SD20* and *SD20-fit* from a combination of *S07* and *DM18*.

Model	Equation	Method	Site	Calibrated range
CC98	$k_{600} = 2.07 + 0.215 \cdot U_{10}^{1.7}$ $k_{Sc} = k_{600}\left(\frac{Sc}{600}\right)^{-1/2}$	Mass Balance By gas tracer	Lake	Area (0.15 km^2) U_{10} (< 9 ms^{-1})
CW03	$k_{600} = 0.168 + 0.228 \cdot U_{10}^{2.2}$ $k_{Sc} = k_{600}\left(\frac{Sc}{600}\right)^{-1/2}$	Mass Balance By gas tracer	Lake	Area (0.128 km^2) U_{10} (< 6 ms^{-1})
VP13	$k_{600} = 2.51 + (1.48 \cdot U_{10}) + (0.39 \cdot U_{10} \cdot log10(Lake\ size)$ $k_{Sc} = k_{600}\left(\frac{Sc}{600}\right)^{-1/2}$	Floating Chamber	Lakes	Area (0.2–602 km^2) U_{10} (< 6 ms^{-1})
T14	$k_{Sc} = a_1 \cdot (\varepsilon \cdot \upsilon)^{1/4} \cdot Sc^{-1/2}$ $\varepsilon = \varepsilon_{Wind\ shear\ +\ Convection}$	Microstructure profiling	Lake	Area (4 km^2) U_{10} (< 10 ms^{-1})
R12	$k_{Sc} = a_1 \cdot (\varepsilon \cdot \upsilon)^{1/4} \cdot Sc^{-1/2}$ $\varepsilon = \varepsilon_{Wind\ shear} + \varepsilon_{Convection}$	-	-	Following *S07*
S07	$k_{Sc} = k_{Sc-NB-S07} + k_{Sc-B-W97}$ $k_{Sc-NB} = a_1 \cdot (\varepsilon \cdot \upsilon)^{1/4} \cdot Sc^{-1/2}$ $\varepsilon = \varepsilon_{Wind\ shear} + \varepsilon_{Convection} + \varepsilon_{Wave\ action}$	Eddy covariance	Ocean	Area (>100'000 km^2) U_{10} (< 20 ms^{-1}) Wave (0–10 m)
DM18	$k_{Sc} = (k_{NB} + k_B) \cdot (Sc/600)^{-1/2}$ $k_{NB} = A_{NB} \cdot u_{*,atm}$ $k_B = (A_B / O_s) \cdot u_{*,atm}^{5/3} \cdot (g \cdot H_s)^{2/3}$	Eddy Covariance	Ocean	Area (>100'000 km^2) U_{10} (< 30 ms^{-1}) Wave (1–10 m)
SD20	$k_{Sc} = k_{Sc-NB-S07*} + k_{Sc-B-DM18}$ *Adaptation of $\varepsilon_{Wave\ action}$ for large lake	Floating Chamber	Lake	Area (582 km^2) U_{10} (< 16 ms^{-1}) Wave (0–1.2 m)
SD20-fit	$k_{Sc} = k_{Sc-NB-S07*} + k_{Sc-B-DM18}$ with a_1 from $k_{Sc-NB-S07*}$ and A_B from $k_{Sc-B-DM18}$ fitted to observations	-	-	-

***CC98* Cole and Caraco (1998), *CW03* Crusius and Wanninkhof (2003), *VP13* Vachon and Prairie (2013), *T14* Tedford et al. (2014), *R12* Read et al. (2012), *S07* Soloviev et al. (2007), *DM18* Deike and Melville (2018).**

https://doi.org/10.5194/esd-2021-30
Preprint. Discussion started: 7 May 2021

Earth System Dynamics Discussions

Table 2: RMSE of k_{600} models for all wind speed (U_{10}), $U_{10} < 5$ m s^{-1} (i.e., LW) and $U_{10} \geq 5$ m s^{-1} (i.e., SW).

RMSE	*CC98*	*CW03*	*VP13*	*T14*	*R12*	*S07*	*DM18*	*SD20*	*SD20-fit*
All U_{10}	9.8	6.5	6.7	8.6	7.5	6.2	7.3	6.2	5.2
$U_{10} < 5$ ms^{-1}	3.2	4.2	4.5	2.9	3.3	3.3	3.5	3.3	3.2
$U_{10} \geq 5$ ms^{-1}	22.8	12.8	12.7	19.8	16.6	13	15.9	13.1	10.5

695

Table 3: Monthly to annual CO_2 flux estimation (mmolC m^{-2} d^{-1}) from *k*-models and monthly ΔCO_2 average (µatm) as well as their deviation from *SD20-fit*.

Period	*ΔCO₂*	*CC98*	*CW03*	*VP13*	*T14*	*R12*	*S07*	*DM18*	*SD20*	*SD20-fit*
April	42	2.7	2.3	6.7	3.3	2.9	3.0	2.7	3.0	3.7
May	-110	-10.0	-16.1	-25.2	-13.2	-13.3	-15.2	-13.2	-13.5	-16.8
June	-85	-5.0	-4.3	-12.7	-6.3	-5.8	-6.0	-5.7	-6.0	-7.3
Spring	**-51**	**-4.2**	**-5.9**	**-10.5**	**-5.5**	**-5.4**	**-6.2**	**-5.5**	**-5.6**	**-6.9**
July	-120	-8.1	-8.4	-21.0	-11.0	-10.7	-11.3	-10.6	-11.0	-13.5
August	-180	-10.3	-7.4	-27.4	-15.8	-14.7	-15.2	-14.8	-15.2	-18.7
September	-140	-8.7	-9.0	-22.7	-13.3	-13.1	-13.7	-13.0	-13.3	-16.7
Summer	**-145**	**-9.0**	**-8.3**	**-23.7**	**-13.4**	**-12.8**	**-13.4**	**-12.8**	**-13.2**	**-16.3**
October	10	0.6	0.6	1.6	1.0	0.9	1.0	1.0	1.0	1.3
November	450	35.0	42.3	93.3	59.7	59.1	62.7	59.7	63.0	78.0
December	590	51.6	80.6	130.0	82.6	83.9	93.2	84.8	92.6	114.5
Fall	**350**	**29.0**	**41.2**	**74.8**	**47.6**	**47.9**	**52.2**	**48.4**	**52.1**	**64.5**
January	540	40.0	49.7	99.7	64.8	60.9	66.5	60.6	65.5	81.0
February	500	49.3	84.8	123.4	71.4	72.5	82.1	72.8	81.0	100.0
March	385	40.3	56.1	102.3	61.3	60.03	65.5	59.4	63.2	78.1
Winter	**475**	**43.1**	**63.1**	**108.1**	**65.7**	**64.5**	**71.1**	**64.1**	**69.7**	**86.0**
Annual	**157**	**14.7**	**22.5**	**37.1**	**23.6**	**23.4**	**25.9**	**23.5**	**25.7**	**31.8**
Annual gCm^{-2}yr^{-1}	**-**	**64.6**	**98.8**	**163.1**	**103.6**	**102.8**	**113.9**	**103.3**	**113.0**	**139.7**
Deviation from *SD20-fit*	**-**	**-54 %**	**-29 %**	**+17 %**	**-26 %**	**-26 %**	**-18 %**	**-26 %**	**-19 %**	**-**

700

https://doi.org/10.5194/esd-2021-30
Preprint. Discussion started: 7 May 2021

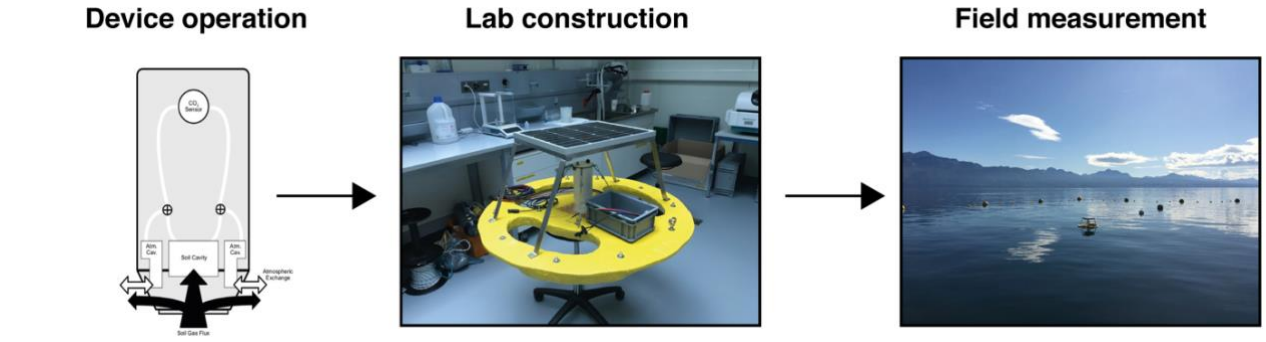

Figure A1: Schematics of eosFD operation (eosense.com) followed by its mini-platform construction and its positioning for measurements in the field (Lake Geneva at LéXPLORE platform). The raft design also complies with recommendations to minimize artificial turbulence induced by the chamber's walls, with 10 cm long-edges entering the water (Vachon et al., 2010).

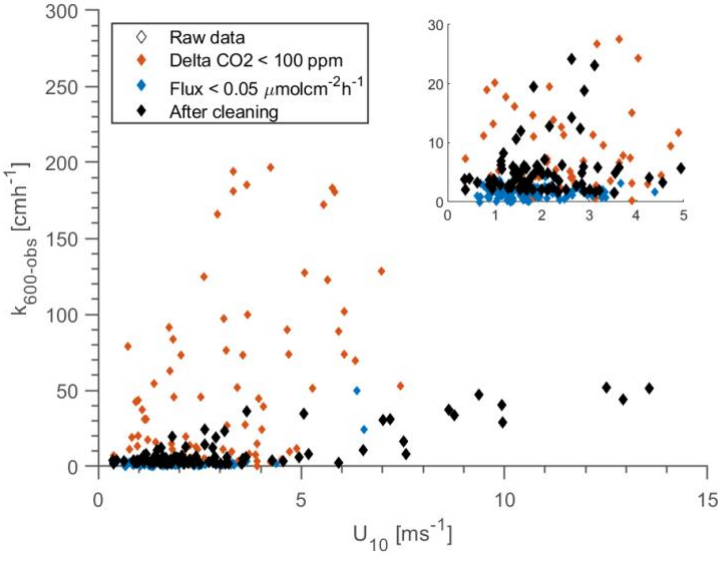

Figure A2: Visualisation of 304 observed k_{600} during the five periods of flux measurements (i.e., 13th–14th June 2019, 27th–28th August 2019, 1st–5th October 2019, 18th–20th December 2019, and 20th–26th February 2020).

https://doi.org/10.5194/esd-2021-30
Preprint. Discussion started: 7 May 2021

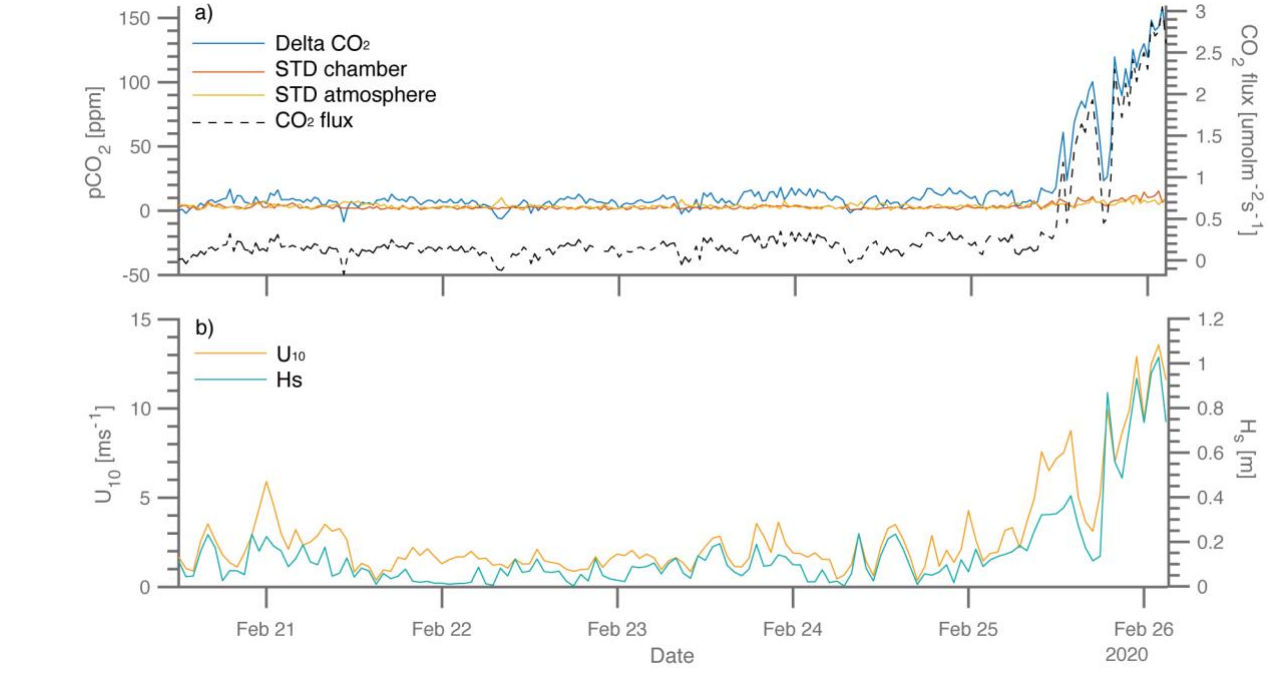

Figure A3: a) Raw outputs of the eosFD during one period of CO_2 flux measurements; ΔCO_2 between both cavities of measures (atmosphere cavity and chamber cavity) (blue line); Standard deviation of each cavity between two automated flushing (30 minutes of interval), Chamber cavity (red line), Atmosphere cavity (yellow line); and the CO_2 flux (black dash line). b) Temporal evolution of U_{10} and H_s during the same period than CO_2 flux measurements. Increase in flux on 25th February corresponding to increase in wind speed and waves.

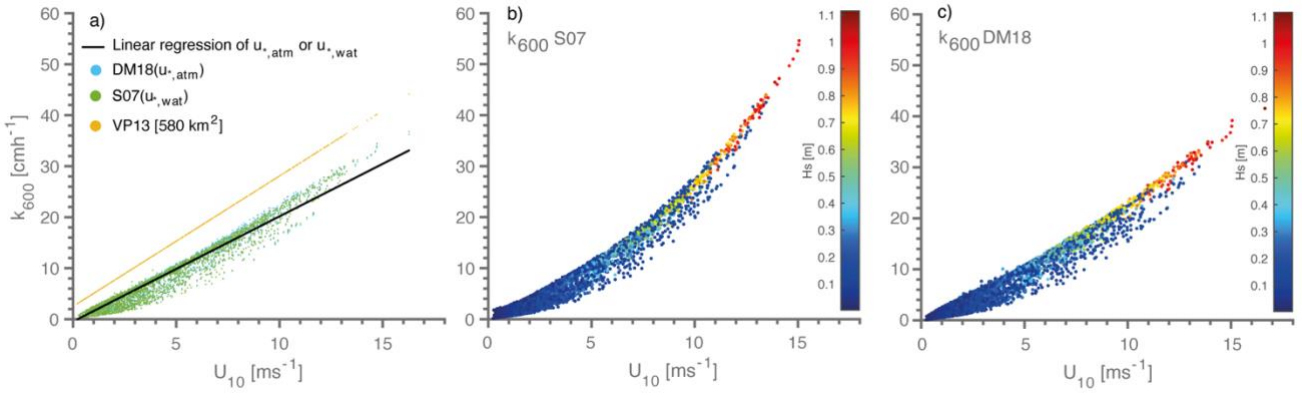

Figure B1: a) Comparison of Soloviev et al. (2007) and Deike and Melville (2018) for the first order function of friction velocity at the water side ($u_{*,wat}$) (blue points) and at the atmosphere side ($u_{*,atm}$) (green points) with their linear regression (black line); the linear function of Vachon and Prairie (2013) for a lake size of 582 km² (yellow points) as well as the linear regression from ; b) Visualisation of *S07* with empirical parameterization of bubble term (Woolf, 1997) regardless of wave height in function of wind speed at 10 m; c) Visualisation of *DM18* in function of wind speed, only effect of bubble term from 10 ms^{-1}.

https://doi.org/10.5194/esd-2021-30
Preprint. Discussion started: 7 May 2021

Earth System Dynamics
Discussions
Open Access
EGU

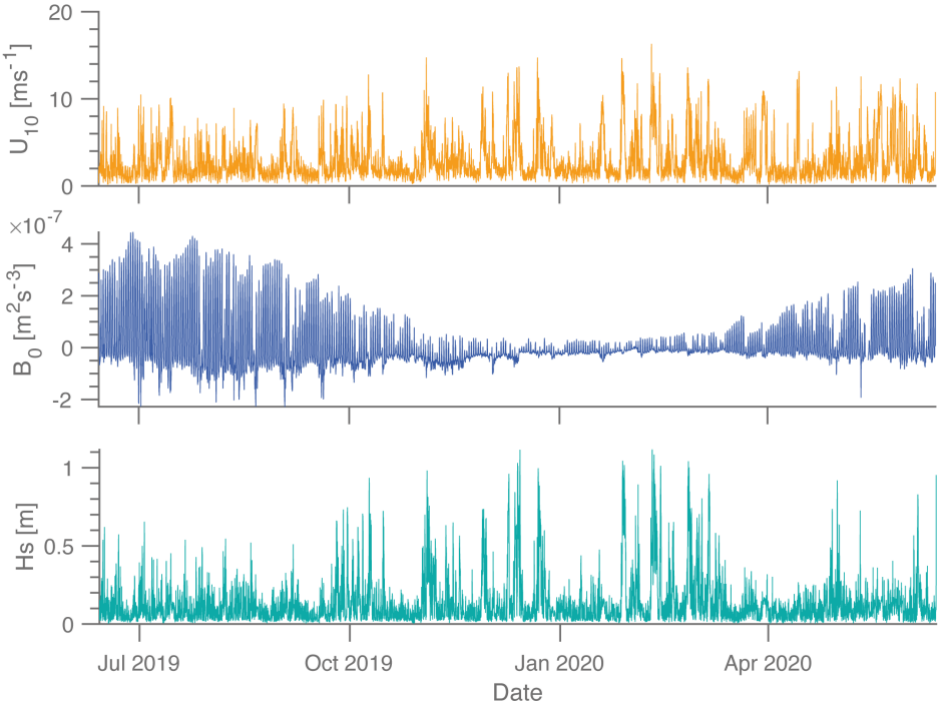

Figure C1: Annual evolution of 3 main inputs of *k*-models; Wind speed at 10 m (U_{10}); Buoyancy flux at surface (B_0); Significant wave height (H_s).